

1 Tau accumulation activates STAT1 triggering memory deficits via suppressing  
2 NMDA receptor expression

3 Xiao-Guang Li<sup>1,4,‡</sup>, Xiao-Yue Hong<sup>1,‡</sup>, Ya-li Wang<sup>1,5</sup>, Shu-Juan Zhang<sup>1</sup>, Jun-Fei Zhang<sup>1</sup>, Xia-  
4 Chun Li<sup>1</sup>, Yan-Chao Liu<sup>1</sup>, Dong-Shen Sun<sup>1</sup>, Qiong Feng<sup>1</sup>, Jin-Wang Ye<sup>1</sup>, Yuan Gao<sup>1</sup>, Dan Ke<sup>1</sup>,  
5 Qun Wang<sup>1</sup>, Hong-lian Li<sup>1</sup>, Keqiang Ye<sup>2</sup>, Gong-Ping Liu<sup>1,3\*</sup>, Jian-Zhi Wang<sup>1,3\*</sup>

6

7 <sup>1</sup>Department of Pathophysiology, School of Basic Medicine and the Collaborative Innovation  
8 Center for Brain Science, Key Laboratory of Ministry of Education of China and Hubei Province  
9 for Neurological Disorders, Tongji Medical College, Huazhong University of Science and  
10 Technology, Wuhan 430030, China.

11 <sup>2</sup>Department of Pathology and Laboratory Medicine, Emory University School of Medicine,  
12 Atlanta, GA 30322, USA.

13 <sup>3</sup>Co-innovation Center of Neuroregeneration, Nantong University, Nantong, JS 226001, China.

14 <sup>4</sup>Clinic Center of Human Gene Research, Union Hospital, Tongji Medical College, Huazhong  
15 University of Science and Technology, Wuhan 430030, China.

16 <sup>5</sup>Department of Physiology and Neurobiology, Key Laboratory for the Brain Research of Henan  
17 Province, Xinxiang Medical University, Xinxiang, PR 453000, China.

18 ‡ X.G.L and X.Y.H. contributed equally to this work.

19 \*Correspondence to: [wangjz@mail.hust.edu.cn](mailto:wangjz@mail.hust.edu.cn) (J.Z.W), and [liugp111@mail.hust.edu.cn](mailto:liugp111@mail.hust.edu.cn)  
20 (G.P.L.).

21 Running title: STAT1 mediates synaptic toxicity of tau

- 22 The number of words in the abstract: 146 words
- 23 The number of words in the text: 6,003 words
- 24 The number of tables: zero
- 25 The number of figures: 7 color figures
- 26 The number of supplementary material: 1 file (3 supplementary table, 11 supplementary figures)

27

28

29

30

31

32

33

34

35

36

37

38

39

40

41

42

43

44

45 **ABSTRACT**

46 Intracellular tau accumulation forming neurofibrillary tangles is hallmark pathology of  
47 Alzheimer's disease (AD), but how tau accumulation induces synapse impairment is elusive. By  
48 overexpressing human full-length wildtype tau (termed hTau) to mimic tau abnormality as seen  
49 in the brain of sporadic AD patients, we found that hTau accumulation activated JAK2 to  
50 phosphorylate STAT1 (Signal Transducer and Activator of Transcription 1) at Tyr701 leading to  
51 STAT1 dimerization, nuclear translocation and its activation. STAT1 activation suppressed  
52 expression of N-methyl-D-aspartate receptors (NMDARs) through direct binding to the specific  
53 GAS element of GluN1, GluN2A and GluN2B promoters, while knockdown STAT1 by AAV-  
54 Cre in STAT1<sup>flox/flox</sup> mice or expressing dominant negative Y701F-STAT1 efficiently rescued  
55 hTau-induced suppression of NMDARs expression with amelioration of synaptic functions and  
56 memory performance. These findings indicate that hTau accumulation impairs synaptic plasticity  
57 through JAK2/STAT1-induced suppression of NMDARs expression, revealing a novel  
58 mechanism for hTau-associated synapse and memory deficits.

59 **Key words:** Tau, STAT1, synapse, N-methyl-D-aspartate receptors, memory.

60

61

62

63

64

65

## 66 INTRODUCTION

67 Intracellular accumulation of tau forming neurofibrillary tangles is one of the two hallmarks in  
68 Alzheimer's disease (AD), the most common neurodegenerative disorder in the elderly [1, 2].  
69 Abnormal tau accumulation is positively correlated with neurodegeneration and memory  
70 deterioration [3, 4], and the total tau level in cerebrospinal fluids has an inverse correlation with  
71 memory score in AD patients [5, 6]. The axonal tau pathology in hippocampus is critical for the  
72 clinical presentation of dementia and may constitute an anatomical substrate of clinically  
73 verifiable memory dysfunctions [3]. The human tau transgenic mice recapitulate features of  
74 human tauopathies and cognitive deficits [7, 8]. Tau is essential for  $\beta$ -amyloid-induced synaptic  
75 toxicity [9], while tau knockout attenuates neuronal dysfunction and prevents behavioral deficits  
76 in transgenic mice expressing human amyloid precursor protein (APP) without altering high A $\beta$   
77 level in the brain [10, 11]. These clinical and laboratory evidence strongly suggest that tau  
78 abnormality plays a pivotal role in AD-like synapse and memory impairments.

79 As a cytoskeleton protein, the originally characterized function of tau is to promote microtubule  
80 assembly and maintain the stability of microtubules, which is essential for axonal transport [12,  
81 13]. Tau hyperphosphorylation dissociates microtubules and thus disrupts axonal transport [14-  
82 18]. Recent studies suggest that tau phosphorylation is actively involved in regulating cell  
83 viability [19-21]. Normally, tau is largely located in the neuronal axons [22]. Upon  
84 hyperphosphorylation [23], tau is located into the dendritic spines where it interacts with the  
85 postsynaptic proteins and thus induces synaptic dysfunction [24, 25]. Intracellular accumulation  
86 of tau causes mitochondrial dysfunction and mitophagy deficits by increasing mitochondrial  
87 membrane potential [26, 27]. Tau accumulation also disrupts intracellular calcium signaling  
88 leading to activation of calcineurin and CREB dephosphorylation in primary neuron cultures [4].

89 These hypothesis-driven studies partially disclose the mechanisms underlying the toxic effects of  
90 tau. However, the molecular mechanism underlying hTau-induced synapse impairment is not  
91 fully understood.

92 In the present study, we employed a large scale screening approach to explore novel molecular  
93 mechanisms underlying tau toxicities. By using whole-genome mRNA chip and the transcription  
94 factor activation profiling array, we found that overexpressing hTau upregulated JAK2/STAT1  
95 signaling, and simultaneous downregulating STAT1 by hippocampal infusion of AAV-Cre in  
96 STAT1<sup>flox/flox</sup> mice or by overexpressing dominant negative STAT1 mutant mitigates the hTau-  
97 induced synaptic and memory deficits. We also found that STAT1 can directly bind to the  
98 specific GAS elements GluN1, GluN2A and GluN2B and thus suppress expression of the  
99 NMDARs, which reveals a novel mechanism underlying hTau-induced synapse impairment and  
100 memory deficit.

101

102

103

104

105

106

## 107 **METHODS AND MATERIALS**

### 108 **Antibodies and reagents**

109 The antibodies used in the present study were listed in the Supplementary Table 3. Itacitinib  
110 (JAK1 inhibitor, from MCE), TG-101348 (special JAK2 inhibitor, from  
111 MCE), JAK2 siRNA (sc-39099, from Santa Cruz), AG490 (JAK2 inhibitor, from Santa Cruz),  
112 SP600125 (the inhibitor of JNK1, from Santa Cruz) and FR180204 (the inhibitor of ERK1, from  
113 Santa Cruz) were purchased. Human pIRES-eGFP-hTau plasmid was a gift of Dr. Khalid Iqbal  
114 (New York State Institute for Basic Research in Developmental Disabilities, Staten Island, NY).  
115 WT-STAT1 and Y701F-STAT1 plasmids were gift of Dr. Xiao-Yuan Li (Institute of Biomedical  
116 Sciences, Academia Sinica, Taiwan).

### 117 **Animals**

118 Male C57 mice were purchased from the animal center of Tongji Medical College, Huazhong  
119 University of Science and Technology. STAT1<sup>flox/flox</sup> (signal transducer and activator of  
120 transcription 1) mutant mice (B6; 129S-STAT1<sup>tm1Mam/Mmjax</sup>) and hTau transgenic mice  
121 (STOCK Mapt<sup>tm1(EGFP)</sup> Klt Tg(MAPT)<sup>8cPdav/J</sup>) were purchased from Jackson lab. All mice  
122 were kept at 24 ± 2 °C on daily 12 h light-dark cycles with ad libitum access to food and water.  
123 All animal experiments were performed according to the ‘Policies on the Use of Animals and  
124 Humans in Neuroscience Research’ revised and approved by the Society for Neuroscience in  
125 1995, and the Guidelines for the Care and Use of Laboratory Animals of the Ministry of Science  
126 and Technology of the People’s Republic of China, and the Institutional Animal Care and Use  
127 Committee at Tongji Medical College, Huazhong University of Science and Technology  
128 approved the study protocol.

## 129 **Stereotaxic brain injection**

130 Adeno-associated virus-eGFP expressing human full-length tau or the control eGFP AAV  
131 (eGFP), AAV-Cre (Cre) and AAV-Y701F-STAT1 virus were purchased from OBio Biologic  
132 Technology Co., Ltd. The titer of the AAV-hTau or its control virus was  $1.13 \times 10^{13}$  v.g./ml,  
133 AAV Cre or AAV-Y701F-STAT1 was  $5 \times 10^{12}$  v.g./ml, and Syn-hTau-AAV was  $1.99 \times 10^{13}$   
134 v.g./ml. The *in vivo* overexpression efficiency was measured by immunohistochemical staining  
135 and Western blotting after injection of the virus into the hippocampal CA3 of mice brains for 1  
136 month. For brain injections, ~3 m-old C57 or STAT1flox/flox mice were positioned respectively  
137 in a stereotaxic instrument, then the virus was bilaterally injected into the hippocampal CA3  
138 region (AP  $\pm 2.0$ , ML -1.5, DV -2.0) at a rate of 0.10  $\mu$ l/min. The needle syringe was left in place  
139 for ~3 min before being withdrawn. The injection did not significantly increase the death rate or  
140 change the normal activity of the mice compared with the non-injected controls. The  
141 hippocampal CA3 region which infected with the virus was used for the biochemical  
142 measurements.

## 143 **Behavioral tests**

144 Four weeks after brain infusion of the viral vectors, the spatial learning and memory were  
145 assessed by Morris water maze (MWM) test [28]. For spatial learning, mice were trained in  
146 water maze to find a hidden platform for 5 consecutive days, 4 trials per day with a 30 s interval  
147 from 14:00 to 20:00 pm. On each trial, the mice started from one of the four quadrants facing the  
148 wall of the pool and ended when the animal climbed on the platform. If the mice did not locate  
149 the platform within 60 s, they were guided to the platform. The swimming path and the time used  
150 to find the platform (latency) or pass through the previous platform quadrant were recorded each  
151 day by a video camera fixed to the ceiling, 1.5 m from the water surface. The camera was

152 connected to a digital-tracking device attached to an IBM computer. The spatial memory was  
153 tested 1 day after the last training. The longer a mouse stayed in the previous platform-located  
154 quadrant, the better it scored the spatial memory.

155 The fear conditioning test was performed as the procedures established in our lab [29]. Briefly,  
156 the mouse was kept in the cage for 3 min to adapt to the environment before experiments, and  
157 then the mice received training by subjecting to 3 min unsignaled foot-shocks (one shock at the  
158 first min, three shocks at the second min and 8 shocks at the third min; 0.5 mA, 2-sec duration,  
159 and 1 min apart). The short-term memory (STM) and long-term memory (LTM) were tested  
160 respectively in 2 h and 24 h after the training by subjecting back into the conditioning chamber  
161 for 3 min and measuring the freezing time.

### 162 **Electrophysiological analysis**

163 Horizontal brain slices (400  $\mu\text{m}$ ) containing the dorsal hippocampus were cut at 4-5  $^{\circ}\text{C}$  in  
164 artificial cerebrospinal fluid (aCSF) consisting of (in mM): 126 NaCl, 3 KCl, 1.25  $\text{NaH}_2\text{PO}_4$ , 24  
165  $\text{NaHCO}_3$ , 2  $\text{MgSO}_4$ , 2  $\text{CaCl}_2$  and 10 glucose (pH 7.4; 305 mOsm), and saturated with carbogen  
166 (95%  $\text{O}_2$  and 5%  $\text{CO}_2$ ), using a Leica VT1000S vibratome (Milton Keynes, UK). Immediately  
167 after slicing sections were transferred and maintained in an interface chamber continuously  
168 perfused with aCSF. The slices were allowed to equilibrate at least for 30 min prior to recording  
169 at room temperature.

170 For extracellular recordings, slices were placed in the interface recording chamber at 32  $^{\circ}\text{C}$  and  
171 the perfusion rate was normally 3 ml/min, while maintaining a thin film of aCSF covering the  
172 slice to make sure applied substances could diffuse into the area recorded. Field potentials were  
173 amplified with Neurolog AC-coupled NL 104 preamplifiers (Digitimer Ltd, Welwyn, UK). The  
174 excitatory postsynaptic potential (fEPSP) was recorded by a 0.1-M $\Omega$  tungsten monopolar



175 electrode from the dendritic layer of the stratum radiatum of the CA3 field following electrical  
176 stimulation of the mossy-fiber pathway. The electrical pulses were delivered using a bipolar  
177 platinum/iridium electrode (25  $\mu$ m wire-diameter, at an inter-wire distance of 100  $\mu$ m, World  
178 Precision Instruments, USA). The fEPSP was quantified by 30 % of the maximum slope of its  
179 rising phase. Input/output (I/O) curves were constructed by measuring fEPSP slopes responding  
180 to the stimulus intensity increasing from 1 to 10 V, with a 0.5-V increment in each slice. Paired-  
181 pulse facilitation (PPF) was examined by applying pairs of pulses, which were separated by 20–  
182 500 ms intervals.

183 For induction of long-term potentiation (LTP), we used theta-burst stimulation (TBS) that  
184 consisted of 4 pulses at 100 Hz, repeated 3 times with a 200-ms interval. The magnitudes of LTP  
185 are expressed as the mean percentage of baseline fEPSP initial slope.

186 NMDA/AMPA receptor EPSC analysis was performed by patch clamp in the presence of 50  $\mu$ M  
187 picrotoxin. The evoked EPSCs were collected at two holding potentials. At -70 mV, responses  
188 were collected and the peak amplitude identified as the AMPA receptor-mediated response. Cells  
189 were then voltage clamped at +40 mV, and the amplitude of the evoked EPSC 50 ms post-  
190 stimulus was identified as the NMDAR-mediated response. Six to eight traces were collected at  
191 0.1 Hz for each membrane potential [30-31].

## 192 **Cell culture**

193 The human embryonic kidney293 (HEK293) were grown in Dulbecco's Modified Eagle's  
194 medium (DMEM), supplemented with 10% (v/v) fetal bovine serum and 1%  
195 penicillin/streptomycin, in a humidified atmosphere containing 5% CO<sub>2</sub> incubator at 37 °C. After

196 growing 24 h in plates or flasks, the cells were transfected with the indicated plasmid(s) using  
197 Lipofectamine2000 according to the manufacturer's instructions.

198 For primary neuron cultures, 18 days embryonic (E18) rat hippocampus were seeded at 30,000-  
199 40,000 cells per well on 6-well plates coated with Poly-D-Lysine/Laminin (Bioscience) in  
200 neurobasal medium (Invitrogen) supplemented with 2% B27/0.5 mM glutamine/25 mM  
201 glutamate. Half the culture medium was changed every 3 days with neurobasal medium  
202 supplemented with 2% B27 and 0.5 mM glutamine. All cultures were kept at 37 °C in a  
203 humidified 5% CO<sub>2</sub> containing atmosphere. More than 90% of the cells were neurons after they  
204 were cultured for 7 to 17 div; this was verified by positive staining for the neuronal specific  
205 markers microtubule-associated protein-2 (MAP2, dendritic marker, Millipore).

#### 206 **Preparation of nuclear fractionation**

207 The nuclear extracts were prepared using the nuclear extraction kit according to the  
208 manufacturer's instructions (Signosis, Inc., Sunnyvale, CA). Briefly, culture dish was added with  
209 Buffer I working reagent and rocked at 200 rpm for 10 min on a shaking platform at 4 °C. The  
210 HEK293 cells were collected and centrifuged at 12,000rpm for 5 min at 4 °C. The supernatant  
211 was discarded, and the pellets were re-suspended by adding Buffer II working reagents. For  
212 tissues, the hippocampal CA3 areas (where virus infected) were rapidly cut into small pieces,  
213 added Buffer I working reagent, and homogenized on ice until a single cell suspension observed  
214 (by microscope). After spun at 500 g for 5 min at 4 °C, the supernatant was removed, and the cell  
215 pellets re-suspended with Buffer I working reagent and rocked at 200 rpm for 10 min on a  
216 shaking platform at 4 °C. Then the cells centrifuged at 10,000 rpm for 5 min at 4 °C, and the  
217 pellets were re-suspended by adding Buffer II working reagents. Lastly, the cell lysis was shaken

218 at 200 rpm on a platform for two hours at 4 °C. After centrifuged at 12,000 rpm for 5 min at 4 °C,  
219 the supernatant (nuclear extract) was collected and stored at -80 °C until use.

### 220 **Preparation of insoluble tau**

221 Insoluble tau aggregates were isolated from virus infected hippocampal tissue by a modified  
222 procedure. Brain tissues were homogenized in lysis buffer (10 mM Tris-HCl, 150 mM NaCl, 20  
223 mM NaF, 1 mM Na<sub>3</sub>VO<sub>4</sub>, 2 mM EGTA, 0.5% Triton X-100, and 0.1% SDS) with protease  
224 inhibitor mixture and centrifuged for 20 min at 13,000 × g. The resulting supernatant designated  
225 as soluble tau fraction. The pellet was resuspended in 1% SDS buffer with 10 times ultrasonic  
226 and designated as insoluble aggregated tau.

### 227 **Western blotting**

228 Equal amounts of protein were separated by 10% sodium dodecyl sulfate-polyacrylamide gel  
229 electrophoresis (SDS-PAGE) and transferred onto nitrocellulose membranes. For analysis of  
230 STAT1 dimerization, cell lysates were incubated for 20 min with 1 mM DSS, blocked with 0.5  
231 mM NH<sub>4</sub>OH, and used for Western blotting with anti-STAT1 antibody [32]. The membranes  
232 were blocked in 5% non-fat milk for 1 h at room temperature and then incubated with primary  
233 antibody (Supplementary Table 3) at 4 °C overnight. Then the blots were incubated with IRDye  
234 800CW-conjugated affinity-purified anti-mouse IgG (Rockland) or IRDye 800CW anti-rabbit  
235 IgG secondary antibody (Rockland) for 1 h at room temperature. Immunoreactive bands were  
236 visualized using Odyssey Infrared Imaging System (Licor Biosciences, Lincoln, NE, USA).

### 237 **Reverse transcription and real-time quantitative PCR**

238 Reverse transcription and real-time quantitative PCR were carried out according to  
239 manufacturer's instruction (TaKaRa, Dalian, China). The PCR system contains 3 mM MgCl<sub>2</sub>,

240 0.5  $\mu$ M forward and reverse primers, 2  $\mu$ l SYBR Green PCR master mixes and 2  $\mu$ l cDNA, and  
241 the standards for each gene were prepared using appropriate primers by a conventional PCR. The  
242 samples were assayed on a Rotor Gene 300 Real-time Cycler (Corbett Research, Sydney,  
243 Australia). The expression level of the interest gene was normalized by the housekeeping gene  
244 glyceraldehyde-3-phosphate dehydrogenase (GAPDH), which was not changed by the  
245 treatments. PCR primers employed in the present study are as follow: Mmu-GluA1 forward and  
246 reverse primers, 5'-CAATGACCGCTATGAGGG-3' and 5'- AAGGACTGAAACGGCTGA-3';  
247 mmu-GluA2 forward and reverse primers, 5'- GTGTCGCCCATCGAAAGTG-3' and 5'-  
248 AGTAGGCATACTTCCCTTTGGAT-3'; mmu-Syn1 forward and reverse primers, 5'-  
249 AGGACGAGGTGAAAGC-3' and 5'-TCAGTCGGAGAAGAGG-3'; mmu-Syt1 forward and  
250 reverse primers, 5'- CCATAGCCATAGTTGC-3' and 5'-GTTTCAGCATCGTCAT-3'; mmu-  
251 GluN1 forward and reverse primers, 5'- GTCCACCAGACTAAAGA-3' and 5'-  
252 TCCCATCATTCCGT-3'; mmu-GluN2A forward and reverse primers, 5'-  
253 CTTTTGAGGACGCC-3' and 5'- AAATGAGACCCGATG-3'; mmu-GluN2B forward and  
254 reverse primers, 5'- GGCTGACTGGCTACG-3' and 5'- CTTGGGCTCAGGGAT-3'; mmu-  
255 GAPDH forward primer 5'-GGAGCGAGATCCCTCCAAAAT-3' and reverse primer 5'-  
256 GGCTGTTGTCATACTTCTCATGG-3'.

### 257 **Transcription factor activating profiling assay**

258 Analysis of the activity of 96 transcription factors (TFs, shown in Supplementary Table 1 and 2)  
259 was performed according to the manufacturer's instructions by using the TF Activation Profiling  
260 Plate Array II (Signosis, Inc., Sunnyvale, CA). HEK293 cells were transfected with tau plasmid  
261 or its control vector for 48 h, and then, the nuclear protein extracts were prepared according to

262 the manufacturer's instructions using the Nuclear Extraction Kit (Signosis, Inc., Sunnyvale, CA).  
263 A 10 µg sample of nuclear protein extracts was assayed per sample.

#### 264 **Electrophoresis mobility shift assay (EMSA)**

265 The Non-radioactive EMSA-STAT1 Kit was purchased from Signosis (Sunnyvale, CA). EMSA  
266 was performed according the protocol supplied by the manufacturer. Briefly, samples were  
267 incubated with a biotinized oligonucleotide probe containing a STAT1 binding site. After  
268 incubation, the samples were separated on a non-denaturing polyacrylamide gel and transferred  
269 to nylon membranes. The transferred oligonucleotides were immobilized by UV crosslinking.  
270 For detection of the oligonucleotides, Streptavidin-HRP was added to the membrane, and the  
271 blots were developed by ECL according to manufacturers' instructions. Competition experiment  
272 was performed using excess amounts of unlabeled cold probe containing STAT1 binding site.

#### 273 **Luciferase reporter assay**

274 Activity of the transcription factors (TFs) was analyzed by using specific luciferase reporter  
275 vectors, including pSTAT1-Luc, pCBF-Luc, pPIT1-Luc, pHNF1-Luc, pHOX4C-Luc and pSF1-  
276 Luc, respectively (Signosis). These vectors contain a cis-element (DNA binding sequence), a  
277 minimal promoter, and a firefly luciferase gene. The activated transcription factors (such as  
278 STAT1, CBF, PIT1, HNF1, HOX4C, and SF1) bind to the cis-element and trans-activate the  
279 expression of the luciferase gene correlating with the measured luciferase enzyme activity.  
280 Therefore, the luciferase activity in this assay represents activation of the transcription factor.  
281 Briefly, the HEK293 cells were transfected with tau plasmid or its empty vector control in  
282 combination with pSTAT1-Luc (or pCBF-Luc, or pPIT1-Luc, or pHNF1-Luc, or pHOX4C-Luc,  
283 or pSF1-Luc) reporter construct and pRL-TK for 48 h. Then the cells were washed with PBS and  
284 lysed in 100 µl of the 1×CCLR (Promega). The luciferase activity was measured by following

285 the manufacture's instruction (Promega). The activity of TFs (i.e. firefly luciferase) was  
286 normalized to transfection efficiency by using Renilla luciferase activity (pRL-TK).

287 To generate luciferase reporter plasmids of GluN1, GluN2A or GluN2B promoter, PCR  
288 fragments (Fig. 5) from the mouse genomic DNA were inserted into the BglIII and NcoI sites of  
289 the pGL3 basic luciferase expression vector (Promega, Madison, WI). Mutation of the pGL3-  
290 GluN1/GluN2A/GluN2B luciferase plasmid was introduced using the GeneTailor system  
291 (Invitrogen). HEK293 cells were transfected with luciferase reporter plasmids using  
292 Lipofectamine Plus (Invitrogen) according to the instructions provided by the manufacturer. To  
293 assay the luciferase activity, HEK293 cells were seeded into 24-well plates in DMEM, one day  
294 prior to transfection, and co-transfected with pGL3-construct, tau and pRL-TK plasmid. After 24  
295 h, cells were harvested and lysed with 100  $\mu$ l Passive Lysis Buffer. The cell extracts (20  $\mu$ l) were  
296 used for luciferase activity assay using a Lumat LB9507 luminometer (Berthold) and the Dual  
297 Luciferase Reporter (DLR) assay system (Promega).

### 298 **Chromatin immunoprecipitation (ChIP) assay**

299 The DNA and protein were cross-linked with 1% formaldehyde for 10 min, washed, and scraped  
300 into cold PBS with protease inhibitors. After centrifugation, the cell pellet was re-suspended in  
301 buffer (20 mM HEPES, pH 7.9, 25 % glycerol, 420 mM NaCl, 1.5 mM MgCl<sub>2</sub>, 0.2 mM EDTA,  
302 protease inhibitors), incubated on ice for 20 min, and centrifuged. The pellet (nucleus) was re-  
303 suspended in breaking buffer (50 mM Tris-HCl, pH 8.0, 1 mM EDTA, 150 mM NaCl, 1 % SDS,  
304 2 % Triton X-100, protease inhibitors) and sonicated 5~10 s, and Triton buffer was added (50  
305 mM Tris-HCl, pH 8.0, 1 mM EDTA, 150 mM NaCl, 0.1% Triton X-100). An aliquot was  
306 reserved as the input, and the remainder was divided to immunoprecipitate with control mouse  
307 IgG (Milipore) or STAT1 (Abcam) antibody followed by incubation with protein G beads.

308 Samples were washed three times in Triton buffer, SDS buffer was added (62.5 mM Tris-HCl,  
309 pH6.8, 200 mM NaCl, 2 % SDS, 10 mM DTT, 2  $\mu$ l of proteinase K (40 mg/ml)), and then  
310 samples were vortexed and incubated at 65 °C overnight to reverse cross-linking. DNA was  
311 isolated using phenol/chloroform extraction and re-suspended in distilled H<sub>2</sub>O. Primers used for  
312 ChIP PCR were as follows: GluN1 forward and reverse primer, 5'-  
313 TAGCATTGGCATTGACCC-3', 5'- GCTGGTGCGGTGATGTGA-3'; GluN2A forward and  
314 reverse primer, 5'- TCGGCTTGGACTGATACGTG-3', 5'- AGGATAGACTGCCCTGCAC-  
315 3'; GluN2B forward and reverse primer, 5'- TCTCCACCGTGCTGATGT-3', 5'-  
316 CTCTCCGAGTCTACCTGTTC-3'. PCR products were analyzed by 2% agarose gel  
317 electrophoresis.

### 318 **Human brain tissue**

319 Fixed AD (n=6, age 80 $\pm$ 7) and the age-matched control (n=5, age 78 $\pm$ 5) brains (kind gifts of Dr.  
320 Iqbal from the NYS Institute for Basic Research, USA) were cut into sections (40  $\mu$ m) with a  
321 freezing microtome (Leitz,Wetzler, Germany; Kryostat 1720) after anhydration in 25 % sucrose  
322 to sinking. The study was approved by the Biospecimen Committee. AD was diagnosed  
323 according to the criteria of the Consortium to Establish a Registry for AD and the National  
324 Institute on Aging. Diagnoses were confirmed by the presence of amyloid plaques and  
325 neurofibrillary tangles in formalin-fixed tissue. Informed consent was obtained from the subjects.

### 326 **Immunohistochemistry**

327 In brief, mice were sacrificed by overdose chloral hydrate (1 g/kg) and perfused through aorta  
328 with 100 ml 0.9 % NaCl followed by 400 ml phosphate buffer containing 4 % paraformaldehyde.  
329 Brains were removed and postfixed in perfusate overnight and then cut into sections (20  $\mu$ m)  
330 with a vibratome (Leica, Nussloch, Germany; S100, TPI). The sections of mice and AD brains

331 were collected consecutively in PBS for immunohistochemistry. Free floating sections were  
332 blocked with 0.3% H<sub>2</sub>O<sub>2</sub> in absolute ethanol for 30 min and nonspecific sites were blocked with  
333 bovine serum albumin (BSA) for another 30 min at room temperature. Sections were then  
334 incubated overnight at 4 °C with primary antibodies. Immunoreaction was developed using  
335 Histostain<sup>TM</sup>-SP kits and visualized with diaminobenzidine (brown color). Sections were  
336 counterstained with hematoxylin, dehydrated through a graded ethanol series, mounted on glass  
337 slides, and sealed with glass coverslips. For each primary antibody, 3-5 consecutive sections  
338 from each brain were used. The images were observed using a microscope (Olympus BX60,  
339 Tokyo, Japan).

#### 340 **Statistical analysis**

341 All data were collected and analyzed in a blinded manner. Data were expressed as mean ± SD or  
342 mean ± SEM and analyzed using SPSS 12.0 statistical software (SPSS Inc. Chicago, IL, USA).  
343 Statistical analysis was performed using student's t-test (two-group comparison), two-way  
344 ANOVA or two-way ANOVA followed by Bonferroni's post hoc test. The level of significance  
345 was set at p<0.05. Image pro-plus software was used to calculate fluorescence intensity of  
346 STAT1 in nucleus on HEK293 cell staining and immunohistochemical staining intensity of  
347 STAT1/pY-STAT1 on human brain slice.

348

349

350



## 351 **RESULTS**

### 352 **Intracellular hTau accumulation induces activation of STAT1**

353 During our studies on tau, we often observe that overexpressing hTau proteins result in changes  
354 of other proteins. We thus speculate that hTau accumulation may influence gene expression. To  
355 test this, we first conducted a whole-genome mRNA chip screening. Indeed, we detected  
356 significant alternations in the level of 520 mRNA molecules (235 increased and 285 decreased)  
357 in hTau-expressing cells compared with those expressing the empty vector (Fig. S1), suggesting  
358 that intracellular hTau accumulation indeed influences gene transcription. To confirm this point,  
359 we measured activity of the transcription factors in nuclear fraction by Transcription Factor  
360 Activation Profiling Array (Table S1 and Table S2), in which the activity of 96 transcription  
361 factors were monitored using a collection of biotin-labeled DNA probes based on the consensus  
362 sequences of individual transcription factor DNA binding sites (Signosis). The results showed  
363 that the activity of STAT1 and CBF was significantly increased, while the activity of HNF1,  
364 HOX4C, PLAG1, SMUC, VDR, SF-1 and PIT1 decreased remarkably in cells overexpressing  
365 hTau (Fig. 1A, B). In protein level measured by Western blotting, only elevation of STAT1 but  
366 not CBF was shown in total extracts and the nuclear fraction (Fig. S2).

367 Herein, we focused on STAT1 which has been implicated in cognitive functions [33, 34]. We  
368 demonstrated that overexpressing hTau remarkably increased the activation-dependent  
369 phosphorylation of STAT1 at Tyr701 (pY-STAT1) in both cell lysates (Fig. 1C, D) and the  
370 nuclear fraction (Fig. 1E, F) with an enhanced nuclear translocation (Fig. 1G) and dimerization  
371 (Fig. 1H) of STAT1 measured by Western blotting and immunofluorescence imaging. Activation  
372 of STAT1 by overexpressing hTau was also detected by TFs luciferase assay (Fig. 1I). By  
373 EMSA assay using an oligonucleotide probe containing STAT1 binding site, we also found that

374 hTau accumulation increased binding of STAT1 to DNA and this association was disrupted by  
375 using cold probe (Fig. 1J). These *in vitro* data indicate that intracellular hTau accumulation  
376 induces STAT1 activation.

377 To test the *in vivo* effects of hTau accumulation on STAT1, we first injected stereotaxically  
378 AAV- hTau into the mouse hippocampi and measured the alterations of STAT1 and pY-STAT1  
379 after 1 month. Expression of hTau was confirmed by Western blotting (Fig. 2A), and fluorescent  
380 imaging and as well as immunohistochemistry (Fig. S3A). Overexpression of hTau significantly  
381 increased total STAT1 and pY-STAT1 in hippocampal extracts and the nuclear fraction (Fig. 2A,  
382 B) without changing VDR, PLAG1 and SMUC (Fig. S3B), suggesting a relatively specific effect  
383 of hTau on STAT1. Infection of control AAV-eGFP did not activate STAT1 (Fig. S3C). By co-  
384 staining of nuclear translocation of STAT1 with NeuN, IBA1 and GFAP, we found that the  
385 neuronal staining of STAT1 was most significant (Fig. S4). Elevation of STAT1 and pY-STAT1  
386 was also detected in the hippocampi of 9 m- and 12 m-old hTau transgenic mice (Fig. 2C, D, Fig.  
387 S5A). By transfecting Syn-hTau-AAV into the hippocampus, we found that the neuron-specific  
388 overexpression of hTau also significantly increased total STAT1 and pY-STAT1 in hippocampal  
389 extracts and the nuclear fraction (Fig. S6A, B). In the cortex of AD patients, both total and pY-  
390 STAT1 in the nucleus were also significantly increased (Fig. 2E, F). These data provide the *in*  
391 *vivo* and human evidence for the role of tau accumulation in activating STAT1.

### 392 **Downregulating STAT1 rescues hTau-induced memory and synaptic deficits**

393 Previous studies show that accumulation of tau in hippocampal CA3 induces spatial learning and  
394 memory deficits in mice [3, 4]. To investigate the role of STAT1 in hTau-induced memory  
395 deficits, we co-injected bilaterally AAV-hTau and AAV-Cre into the hippocampal CA3 of  
396 STAT1<sup>fl<sup>ox</sup>/fl<sup>ox</sup></sup> mice. The efficiency of AAV-Cre in downregulating STAT1 was confirmed by

397 immunohistochemistry and Western blotting (Fig. 3A, B). By MWM test, we observed that  
398 STAT1 knockdown could efficiently rescue the hTau-induced spatial learning impairments  
399 shown by the decreased escape latency at days 4 and 5 during the 5-days training (Fig. 3C). In  
400 memory test measured at day 6 by removed the escape platform, the mice with STAT1  
401 knockdown showed less average latency to reach the previous target quadrant (Fig. 3D), more  
402 frequent crosses in the platform area (Fig. 3E) and more time stayed in the platform quadrant  
403 (Fig. 3F) than the control mice. No significant difference in swimming speed was seen among  
404 the three groups (Fig. 3G), which excluded motor deficits. By fear conditioning test, we also  
405 observed that STAT1 knockdown improved long-term memory shown by an increased freezing  
406 time during memory test in human hTau-expressing mice (Fig. 3H). These data demonstrate that  
407 downregulating STAT1 in hippocampus can efficiently rescue hTau-induced learning and  
408 memory impairments.

409 Synaptic plasticity is the precondition of learning and memory, therefore we studied how hTau  
410 accumulation or with simultaneous STAT1 knockdown affects synaptic functions on the acute  
411 brain slices. Using a paired-pulse protocol to determine the paired-pulse ratios (PPR) of the  
412 fEPSP at mossy fiber-CA3 circuit, we did not find significant difference between AAV-hTau and  
413 AAV-GFP injected mice (Fig. 3J), indicating no significant presynaptic dysfunction. On the  
414 other hand, the fEPSP slope was reduced in hTau-expression slices compared with AAV-GFP  
415 controls, and downregulating STAT1 substantially attenuated the hTau-induced suppression of  
416 LTP (Fig. 3I, K, L). These data indicate that hTau suppresses LTP by preferentially affecting  
417 postsynaptic machineries and knockdown STAT1 can rescue the hTau-induced suppression of  
418 synaptic transmission.

419 Using whole-cell patch clamp recording, we measured NMDA and AMPA receptor-mediated  
420 synaptic responses at DG-CA3 synapses on acute hippocampal slices. AMPA receptor-mediated  
421 responses had no change, while the NMDAR-mediated responses were significantly decreased  
422 with a decreased ratio of NMDA/AMPA in hTau-overexpressing mice, and downregulating  
423 STAT1 substantially attenuated the hTau-induced suppression of NMDAR currents (Fig. 3M-P).  
424 These data provide functional evidence supporting NMDAR impairment by hTau accumulation  
425 in CA3 neurons.

#### 426 **STAT1 suppresses NMDAR expression *via* binding to the specific domain of the promoter**

427 To explore how hTau-induced STAT1 elevation affects synaptic function, we measured the level  
428 of synapse-related proteins. The results showed that hTau accumulation in mice or  
429 overexpression WT-STAT1 in primary hippocampal neurons decreased the protein and mRNA  
430 levels of postsynaptic proteins N-methyl-D-aspartate receptors (NMDARs) type 1 (GluN1),  
431 GluN2A and GluN2B, while knockdown STAT1 by AAV-Cre substantially restored the protein  
432 and mRNA levels of the NMDARs measured respectively by Western blotting (Fig. 4A, B, D, E;  
433 Fig. S7A, B), RT-PCR (Fig. 4C, F; Fig. S7C), and immunohistochemical staining (Fig. S7D, E).  
434 On the other hand, overexpressing hTau with or without STAT1 knockdown did not significantly  
435 affect the protein levels of presynaptic proteins synapsin1 (Syn1) and synaptotagmin1 (Syt1), or  
436 postsynaptic proteins AMPA receptor subunits GluA1 and GluA2 (Fig.4A-F). These data  
437 suggest that STAT1 elevation mediates the hTau-induced suppression of NMDAR expression.  
438 We also found that NMDAR protein levels decreased in the 9 m- and 12 m-old hTau transgenic  
439 mice compared with the wildtype littermates (Fig. S5B). By transfecting Syn-hTau-AAV into the  
440 hippocampus, we found that the Syn-specific neuronal overexpression of hTau also decreased  
441 NMDAR levels (Fig. S6C), as seen in the pan-neuronal overexpression of hTau (Fig. 4A, 4B).

442 To explore how STAT1 suppresses the expression of NMDARs, we screened potential binding  
443 sites of STAT1 in the promoter regions of GluN1, GluN2A and GluN2B in a transcription factor  
444 database [35]. We found 2 conserved GAS promoter elements for STAT1 binding in the  
445 promoter regions of GluN1 and GluN2B, and 4 GAS promoter elements in GluN2A (Fig. 5C, E,  
446 G). Further studies by chromatin immunoprecipitation (CHIP) assay demonstrated that  
447 overexpression of hTau in hippocampus remarkably increased binding of STAT1 to the  
448 promoters of GluN1, GluN2A and GluN2B genes (Fig. 5A), and upregulating wildtype STAT1  
449 inhibited transcription activity of the NMDARs (Fig. 5B). These data together demonstrate that  
450 STAT1 activation can suppress NMDAR expression by direct binding to the promoter.

451 To clarify the specific GAS promoter element of GluN1, GluN2A or GluN2B genes for STAT1,  
452 we constructed luciferase reporters containing various GAS elements on the NMDAR promoters  
453 (Fig. 5C-H). After co-transfection of specific GAS element reporters with STAT1 into HEK293  
454 cells, we found that co-expression of STAT1 with GAS1 on GluN1 (Fig. 5C, D) or GAS2 on  
455 GluN2B (Fig. 5E, F) induced inhibition of luciferase activity, while the luciferase activity of  
456 GAS2 on GluN1 and GAS1 on GluN2B was not changed by STAT1 (Fig. 5D, F). Furthermore,  
457 expression of mutant GAS1 on GluN1 or GAS2 on GluN2B abolished STAT1-induced inhibition  
458 of luciferase activity (Fig. 5D, F). These data suggest that STAT1 inhibits GluN1 and GluN2B  
459 expression by binding to GAS1 (GluN1) and GAS2 (GluN2B) elements, respectively.

460 In case of GluN2A that has 4 GAS elements, we found that co-expression of STAT1 with GAS1,  
461 2 or 4 elements did not change luciferase activity (Fig. 5G, H); but co-expression of STAT1 with  
462 GAS3 element induced transcriptional activation and that was abolished by GAS3 mutant (Fig.  
463 5H). To clarify these conflict results, we did a random assortment study of the reporters. The  
464 results showed that co-expression of GAS1-3, GAS2-4 and GAS3-4 elements with STAT1

465 induced inhibition of luciferase activity, while co-expression of GAS2-3 elements increased the  
466 luciferase activity (Fig. 5I-J). These data suggest that a multi-GASs-dependent binding of  
467 STAT1 may be involved on GluN2A subunit.

468 We also measured laminin  $\beta$ 1 (LB1) that is involved in A $\beta$ -induced suppression of NMDAR  
469 expression [33]. No significant change was detected after overexpressing hTau (Fig. S8),  
470 suggesting that hTau induces synapse impairment with distinct mechanisms from A $\beta$ .

### 471 **JAK2 activation mediates hTau-induced STAT1 upregulation**

472 Phosphorylation of STAT1 is critical for its nuclear translocation and the activation [36]. To  
473 further explore the upstream factors mediating hTau-induced STAT1 activation, we screened  
474 protein kinases that can phosphorylate STAT1 [37, 38]. Among various kinases, JAK2, JNK and  
475 ERK were activated by overexpressing hTau (Fig. 6A, B), while only simultaneous inhibition of  
476 JAK2 by JAK2 inhibitor TG-101348 (JAK2I) or JAK2 siRNA but not JNK or ERK abolished  
477 hTau-induced STAT1 hyperphosphorylation at pY701 in both total cell extracts and the nuclear  
478 fraction (Fig. 6C-J, Fig. S9). JAK2 activation was also detected in hippocampus of 12 m-old  
479 hTau transgenic mice and CMV-hTau-AAV or Syn-hTau-AAV infused C57 mice (Fig. 6K, L  
480 and Fig. S6A). These data demonstrate that hTau accumulation upregulates STAT1 activity by  
481 activating JAK2.

### 482 **Blocking STAT1 activation rescues hTau-induced synapse and memory impairments**

483 To verify the role of STAT1 phosphorylation in regulating expression of NMDARs and the  
484 cognitive ability, we constructed non-phosphorylation STAT1 dominant negative mutant  
485 (Y701F-STAT1) AAV virus and co-infused the mutant virus with AAV-hTau into the  
486 hippocampal CA3 of 3 m-old C57 mice for one month (Fig. 7A). We found that co-expression of

487 dominant negative Y701F-STAT1 attenuated hTau-induced learning and memory deficits (Fig.  
488 7B-F) with attenuation of LTP suppression (Fig. 7G, H) and restoration of GluN1, GluN2A and  
489 GluN2B protein and mRNA levels (Fig. 7I-K). These data reveal that phosphorylation of STAT1  
490 at Tyr701 indeed plays a critical role in hTau-induced synapse and memory impairments.

491 To explore whether STAT1 knockdown affects tau phosphorylation and aggregation, we co-  
492 infused STAT1 dominant negative mutant (AAV-Y701F-STAT1) with AAV-hTau into the  
493 hippocampal CA3 of 3 m-old C57 mice. After one month, the hTau level in soluble and insoluble  
494 fractions of hippocampal CA3 was measured. Reduction of p-hTau (pS214, pT231 and pS404)  
495 was shown in soluble and insoluble fractions, and total tau (Tau-5) protein decreased in insoluble  
496 fractions (Fig. S10). These data suggest that downregulating STAT1 could attenuate hTau-  
497 toxicities by reducing tau hyperphosphorylation and the pathological aggregation.

498

499 **DISCUSSION**

500 Tau accumulation forming neurofibrillary tangles is hallmark of AD pathologies, but how tau  
501 accumulation induces synapse and memory impairment is elusive. By overexpressing hTau to  
502 mimic intraneuronal tau accumulation as seen in the sporadic AD cases, we show that hTau  
503 accumulation activates JAK2 to phosphorylate and activate STAT1. Upregulation of STAT1  
504 subsequently inhibits expression of GluN1, GluN2A and GluN2B by binding to their specific  
505 promoter elements, which results in synaptic dysfunction and memory deficit. We also  
506 demonstrate that knockdown STAT1 by AAV-Cre in STAT1<sup>fl<sup>ox</sup>/fl<sup>ox</sup></sup> mice or by overexpressing  
507 dominant negative AAV-Y701F-STAT1 efficiently rescues hTau-induced suppression of  
508 NMDAR expression with attenuation of synaptic functions and memory performance. These  
509 findings reveal that intracellular accumulation of hTau causes memory deterioration through  
510 JAK2/STAT1-induced suppression of NMDARs expression, which discloses a novel mechanism  
511 for tau-related synapse and memory impairments (Fig. S11).

512 The mammalian STAT family is consisted of seven members, i.e., STAT1, 2, 3 and 4, STAT5a,  
513 STAT5b and STAT6 [39], among them, STAT1, 3, 5 and 6 are differentially expressed in the  
514 brain [40]. Serve as transcription factors, the activity of STATs is regulated by phosphorylation  
515 [41, 42], and phosphorylation of STAT1 at Tyr701 stimulates its dimerization, nuclear  
516 translocation, DNA binding, and activation [36]. By using multiple measures including  
517 phosphorylation, dimerization, EMSA and luciferase activity assay, we provide strong evidence  
518 showing that hTau accumulation can activate STAT1. Furthermore, expression of un-  
519 phosphorylable dominant negative Y701F-STAT1 attenuates hTau-induced suppression of  
520 synaptic plasticity, which confirms a critical role of Tyr701-phosphorylation in regulating  
521 STAT1 activity. In addition to STAT1, we also detected upregulation of CBF and



522 downregulation of seven Tfs in HEK293 cells after overexpressing hTau by transcription factor  
523 activating profiling assay. In the following studies on HEK293 and mouse brain with  
524 overexpression of hTau, some of the results were not recapitulated by Western blotting. This  
525 discrepancy can be caused by different measures (activity *versus* protein level), the experimental  
526 methods and the materials used. By website prediction of the transcription factor binding sites  
527 (<http://gene-regulation.com/pub/programs/alibaba2/index.html>), we also found that in addition to  
528 STAT1, the other Tfs, such as HNF1, HOX4C, and PIT1, also have potential NMDAR binding  
529 element. Therefore, we measured whether overexpressing hTau affect the activity of HNF1,  
530 HOX4C, and PIT1, but no significant change was shown. These data suggest a relatively specific  
531 and significant effect of hTau on STAT1, and consequently the role of STAT1 on NMDARs.

532 Several tyrosine kinases, such as ERK1, JNK1, p38 kinase, MEK1, MSK1 and the JAK kinases,  
533 are involved in STAT1 phosphorylation [37, 38]. Among them, we observed that JAK2, JNK  
534 and ERK were activated upon intracellular hTau accumulation. However, only simultaneous  
535 inhibition of JAK2 but not JNK and ERK abolished the hTau-induced STAT1 phosphorylation,  
536 which suggests a critical role of JAK2 activation in hTau-induced STAT1 activation. The  
537 JAK/STAT pathway is involved in many pathophysiological processes including cell survival,  
538 proliferation, differentiation, development and inflammation. Recent studies show that  
539 overexpression of STAT1 impairs water maze performance in mice [33, 34]. STAT1 can bind to  
540 the promoter of extracellular matrix protein laminin  $\beta$ 1 (LB1), by which it downregulates the  
541 expression of GluN1 and GluN2B in A $\beta$  treatment [33]. These data suggest an indirect role of  
542 STAT1 in regulating NMDARs via LB1. In the present study, we find that STAT1 can directly  
543 bind to the special GAS elements on NMDAR promoters, and thus directly blocks the expression

544 of NMDAR subunits. These data not only reveal novel mechanism underlying the STAT1-  
545 regulation on synaptic function, but also provide potential strategy for intervention.

546 To identify the exact binding element(s) of STAT1 on NMDAR promoters, we constructed GAS  
547 promoter elements (GASs) in NMDAR promoter regions for luciferase activity assay. We  
548 observed that GAS1 in GluN1 promoter and GAS2 in GluN2B promoter were required for  
549 STAT1 negative regulation of the genes expression. However, STAT1 increased luciferase  
550 activity of GAS3-containing constructs in GluN2A promoter, which is inconsistent with the  
551 reduced mRNA and protein levels of GluN2A by STAT1. Our further studies reveal that STAT1  
552 negative regulation of GluN2A promoter needs concomitant effect of GAS3 with GAS1 or  
553 GAS4, suggesting that STAT1-dependent suppression of GluN2A requires a distal promoter  
554 region containing multiple GAS elements. This phenomenon was also seen in IFN $\gamma$ -mediated  
555 transcriptional suppression of the perlecan gene [43]. It is well known that STAT1 plays an  
556 important role in immune response [44], and inhibition of neuroinflammation ameliorates  
557 learning and memory deficits in AD animal models [45-47]. Whether and how inflammation  
558 may be involved in hTau-induced memory deficits deserve further investigation.

559 Taken together, we find here that intracellular accumulation of hTau suppresses NMDAR  
560 expression by activating JAK2/STAT1 signaling pathway, and thus induces synaptic and  
561 memory impairments. Downregulating STAT1 or blocking STAT1 activation efficiently rescues  
562 the hTau-induced synaptic dysfunction and memory impairment in mice.

563

564 **ACKNOWLEDGMENTS**

565 We thank Dr. Xiao-Yuan Li of Institute of Biomedical Sciences, Academia Sinica, Taiwan for  
566 the kind gift of STAT1 plasmids. This work was supported in parts by Natural Science  
567 Foundation of China (81471303, 31730035 and 81801062), and by Ministry of Science and  
568 Technology of China (2016YFC1305800).

569

570 **AUTHOR CONTRIBUTIONS**

571 J.Z.W. and G.P.L. conceived the project, designed the experiments, and wrote the manuscript.  
572 X.G.L and X.Y.H designed and performed most of the experiments. Y.L.W, S.J.Z., and D.S.S.  
573 performed electrophysiological experiments. Q.F., J.W.Y. and Y.G. prepared primary neurons.  
574 H.L.L. performed the immunohistochemical experiments. J.F.Z., X.C.L., Y.C.L., D.K., and Q.W.  
575 assisted with *in vivo* and *in vitro* experiments. K.Y. assisted with data analysis and interpretation  
576 and critically read the manuscript.

577

578

579

580

581

582

583

584

585

586

587

588

589

590 **CONFLICTS OF INTEREST**

591 All authors disclose: (a) no actual or potential conflicts of interest including any financial,  
592 personal or other relationships with other people or organizations within three years of beginning  
593 the work submitted that could inappropriately influence (bias) their work. (b) When applicable,  
594 provide statements verifying that appropriate approval and procedures were used concerning  
595 animals.

596

597

598 **REFERENCES**

- 599 1. Arai H, Lee VM, Otvos L, Jr., Greenberg BD, Lowery DE, Sharma SK et al. Defined  
600 neurofilament, hTau, and beta-amyloid precursor protein epitopes distinguish Alzheimer  
601 from non-Alzheimer senile plaques. *Proceedings of the National Academy of Sciences of*  
602 *the United States of America* 1990; 87(6): 2249-2253.
- 603 2. Braak H, Braak E. Demonstration of amyloid deposits and neurofibrillary changes in whole  
604 brain sections. *Brain pathology* 1991; 1(3): 213-216.
- 605 3. Thal DR, Holzer M, Rub U, Waldmann G, Gunzel S, Zedlick D et al. Alzheimer-related  
606 hTau-pathology in the perforant path target zone and in the hippocampal stratum oriens and  
607 radiatum correlates with onset and degree of dementia. *Experimental neurology* 2000;  
608 163(1): 98-110.
- 609 4. Yin Y, Gao D, Wang Y, Wang ZH, Wang X, Ye J et al. Tau accumulation induces synaptic  
610 impairment and memory deficit by calcineurin-mediated inactivation of nuclear  
611 CaMKIV/CREB signaling. *Proceedings of the National Academy of Sciences of the United*  
612 *States of America* 2016; 113(26): E3773-3781.
- 613 5. Hu YY, He SS, Wang X, Duan QH, Grundke-Iqbal I, Iqbal K et al. Levels of  
614 nonphosphorylated and phosphorylated hTau in cerebrospinal fluid of Alzheimer's disease  
615 patients : an ultrasensitive bienzyme-substrate-recycle enzyme-linked immunosorbent assay.  
616 *The American journal of pathology* 2002; 160(4): 1269-1278.
- 617 6. Lin YT, Cheng JT, Yao YC, Juo, Lo YK, Lin CH et al. Increased total TAU but not  
618 amyloid-beta(42) in cerebrospinal fluid correlates with short-term memory impairment in  
619 Alzheimer's disease. *Journal of Alzheimer's disease : JAD* 2009; 18(4): 907-918.
- 620 7. Kelleher I, Garwood C, Hanger DP, Anderton BH, Noble W. Kinase activities increase

- 621 during the development of hTauopathy in hTau mice. *Journal of neurochemistry* 2007;  
622 103(6): 2256-2267.
- 623 8. Kimura T, Yamashita S, Fukuda T, Park JM, Murayama M, Mizoroki T et al.  
624 Hyperphosphorylated hTau in parahippocampal cortex impairs place learning in aged mice  
625 expressing wild-type human hTau. *The EMBO journal* 2007; 26(24): 5143-5152.
- 626 9. Rapoport M, Dawson HN, Binder LI, Vitek MP, Ferreira A. Tau is essential to beta -  
627 amyloid-induced neurotoxicity. *Proceedings of the National Academy of Sciences of the*  
628 *United States of America* 2002; 99(9): 6364-6369.
- 629 10. Roberson ED, Scarce-Levie K, Palop JJ, Yan F, Cheng IH, Wu T et al. Reducing  
630 endogenous hTau ameliorates amyloid beta-induced deficits in an Alzheimer's disease  
631 mouse model. *Science* 2007; 316(5825): 750-754.
- 632 11. Vossel KA, Xu JC, Fomenko V, Miyamoto T, Suberbielle E, Knox JA et al. Tau reduction  
633 prevents Abeta-induced axonal transport deficits by blocking activation of GSK3beta. *The*  
634 *Journal of cell biology* 2015; 209(3): 419-433.
- 635 12. Weingarten MD, Lockwood AH, Hwo SY, Kirschner MW. A protein factor essential for  
636 microtubule assembly. *Proceedings of the National Academy of Sciences of the United*  
637 *States of America* 1975; 72(5): 1858-1862.
- 638 13. Cleveland DW, Hwo SY, Kirschner MW. Purification of hTau, a microtubule-associated  
639 protein that induces assembly of microtubules from purified tubulin. *Journal of molecular*  
640 *biology* 1977; 116(2): 207-225.
- 641 14. Alonso AC, Zaidi T, Grundke-Iqbal I, Iqbal K. Role of abnormally phosphorylated hTau in  
642 the breakdown of microtubules in Alzheimer disease. *Proceedings of the National Academy*  
643 *of Sciences of the United States of America* 1994; 91(12): 5562-5566.

- 644 15. Ebner A, Godemann R, Stamer K, Illenberger S, Trinczek B, Mandelkow E.  
645 Overexpression of hTau protein inhibits kinesin-dependent trafficking of vesicles,  
646 mitochondria, and endoplasmic reticulum: implications for Alzheimer's disease. *The Journal*  
647 *of cell biology* 1998; 143(3): 777-794.
- 648 16. Kunzi V, Glatzel M, Nakano MY, Greber UF, Van Leuven F, Aguzzi A. Unhampered prion  
649 neuroinvasion despite impaired fast axonal transport in transgenic mice overexpressing four-  
650 repeat hTau. *The Journal of neuroscience : the official journal of the Society for*  
651 *Neuroscience* 2002; 22(17): 7471-7477.
- 652 17. Audouard E, Van Hees L, Suain V, Yilmaz Z, Poncelet L, Leroy K et al. Motor deficit in a  
653 hTauopathy model is induced by disturbances of axonal transport leading to dying-back  
654 degeneration and denervation of neuromuscular junctions. *The American journal of*  
655 *pathology* 2015; 185(10): 2685-2697.
- 656 18. Cox K, Combs B, Abdelmesih B, Morfini G, Brady ST, Kanaan NM. Analysis of isoform-  
657 specific hTau aggregates suggests a common toxic mechanism involving similar  
658 pathological conformations and axonal transport inhibition. *Neurobiology of aging* 2016; 47:  
659 113-126.
- 660 19. Li HL, Wang HH, Liu SJ, Deng YQ, Zhang YJ, Tian Q et al. Phosphorylation of hTau  
661 antagonizes apoptosis by stabilizing beta-catenin, a mechanism involved in Alzheimer's  
662 neurodegeneration. *Proceedings of the National Academy of Sciences of the United States*  
663 *of America* 2007; 104(9): 3591-3596.
- 664 20. Duan DX, Chai GS, Ni ZF, Hu Y, Luo Y, Cheng XS et al. Phosphorylation of hTau by  
665 death-associated protein kinase 1 antagonizes the kinase-induced cell apoptosis. *Journal of*  
666 *Alzheimer's disease : JAD* 2013; 37(4): 795-808.



- 667 21. Luo DJ, Feng Q, Wang ZH, Sun DS, Wang Q, Wang JZ et al. Knockdown of  
668 phosphotyrosyl phosphatase activator induces apoptosis via mitochondrial pathway and the  
669 attenuation by simultaneous hTau hyperphosphorylation. *Journal of neurochemistry* 2014;  
670 130(6): 816-825.
- 671 22. Binder LI, Frankfurter A, Rebhun LI. The distribution of hTau in the mammalian central  
672 nervous system. *The Journal of cell biology* 1985; 101(4): 1371-1378.
- 673 23. Zhao X, Kotilinek LA, Smith B, Hlynialuk C, Zahs K, Ramsden M et al. Caspase-2 cleavage  
674 of hTau reversibly impairs memory. *Nature medicine* 2016; 22(11): 1268-1276.
- 675 24. Thies E, Mandelkow EM. Missorting of hTau in neurons causes degeneration of synapses  
676 that can be rescued by the kinase MARK2/Par-1. *The Journal of neuroscience : the official  
677 journal of the Society for Neuroscience* 2007; 27(11): 2896-2907.
- 678 25. Ittner LM, Ke YD, Delerue F, Bi M, Gladbach A, van Eersel J et al. Dendritic function of  
679 hTau mediates amyloid-beta toxicity in Alzheimer's disease mouse models. *Cell* 2010;  
680 142(3): 387-397.
- 681 26. Hu Y, Li XC, Wang ZH, Luo Y, Zhang X, Liu XP et al. Tau accumulation impairs  
682 mitophagy via increasing mitochondrial membrane potential and reducing mitochondrial  
683 Parkin. *Oncotarget* 2016; 7(14): 17356-17368.
- 684 27. Li XC, Hu Y, Wang ZH, Luo Y, Zhang Y, Liu XP et al. Human wild-type full-length hTau  
685 accumulation disrupts mitochondrial dynamics and the functions via increasing mitofusins.  
686 *Scientific reports* 2016; 6: 24756.
- 687 28. Morris RG, Garrud P, Rawlins JN, O'Keefe J. Place navigation impaired in rats with  
688 hippocampal lesions. *Nature* 1982; 297(5868): 681-683.
- 689 29. Jiang X, Chai GS, Wang ZH, Hu Y, Li XG, Ma ZW et al. CaMKII-dependent dendrite

- 690 ramification and spine generation promote spatial training-induced memory improvement in  
691 a rat model of sporadic Alzheimer's disease. *Neurobiology of aging* 2015; 36(2): 867-876.
- 692 30. Chittajallu, R., Wester, J.C., Craig, M.T., Barksdale, E., Yuan, X.Q., Akgul, G., Fang, C.,  
693 Collins, D., Hunt, S., Pelkey, K.A., et al. (2017). Afferent specific role of NMDA receptors  
694 for the circuit integration of hippocampal neurogliaform cells. *Nature communications* 8,  
695 152.
- 696 31. Etherton, M., Foldy, C., Sharma, M., Tabuchi, K., Liu, X., Shamloo, M., Malenka, R.C., and  
697 Sudhof, T.C. (2011). Autism-linked neuroligin-3 R451C mutation differentially alters  
698 hippocampal and cortical synaptic function. *Proceedings of the National Academy of*  
699 *Sciences of the United States of America* 108, 13764-13769.
- 700 32. Koshelnick Y, Ehart M, Hufnagl P, Heinrich PC, Binder BR. Urokinase receptor is  
701 associated with the components of the JAK1/STAT1 signaling pathway and leads to  
702 activation of this pathway upon receptor clustering in the human kidney epithelial tumor cell  
703 line TCL-598. *The Journal of biological chemistry* 1997; 272(45): 28563-28567.
- 704 33. Hsu WL, Ma YL, Hsieh DY, Liu YC, Lee EH. STAT1 negatively regulates spatial memory  
705 formation and mediates the memory-impairing effect of Abeta. *Neuropsychopharmacology* :  
706 official publication of the American College of Neuropsychopharmacology 2014; 39(3):  
707 746-758.
- 708 34. Tai DJ, Hsu WL, Liu YC, Ma YL, Lee EH. Novel role and mechanism of protein inhibitor  
709 of activated STAT1 in spatial learning. *The EMBO journal* 2011; 30(1): 205-220.
- 710
- 711 35. Sandelin A, Alkema W, Engstrom P, Wasserman WW, Lenhard B. JASPAR: an open-  
712 access database for eukaryotic transcription factor binding profiles. *Nucleic acids research*

- 713 2004; 32(Database issue): D91-94.
- 714 36. Liddle FJ, Alvarez JV, Poli V, Frank DA. Tyrosine phosphorylation is required for  
715 functional activation of disulfide-containing constitutively active STAT mutants.  
716 *Biochemistry* 2006; 45(17): 5599-5605.
- 717 37. Zhang Y, Cho YY, Petersen BL, Zhu F, Dong Z. Evidence of STAT1 phosphorylation  
718 modulated by MAPKs, MEK1 and MSK1. *Carcinogenesis* 2004; 25(7): 1165-1175.
- 719 38. Quelle FW, Thierfelder W, Witthuhn BA, Tang B, Cohen S, Ihle JN. Phosphorylation and  
720 activation of the DNA binding activity of purified Stat1 by the Janus protein-tyrosine  
721 kinases and the epidermal growth factor receptor. *The Journal of biological chemistry* 1995;  
722 270(35): 20775-20780.
- 723 39. Darnell JE, Jr. STATs and gene regulation. *Science* 1997; 277(5332): 1630-1635.
- 724 40. Jatiani SS, Baker SJ, Silverman LR, Reddy EP. Jak/STAT pathways in cytokine signaling  
725 and myeloproliferative disorders: approaches for targeted therapies. *Genes & cancer* 2010;  
726 1(10): 979-993.
- 727 41. Wegenka UM, Buschmann J, Luttkien C, Heinrich PC, Horn F. Acute-phase response  
728 factor, a nuclear factor binding to acute-phase response elements, is rapidly activated by  
729 interleukin-6 at the posttranslational level. *Molecular and cellular biology* 1993; 13(1): 276-  
730 288.
- 731 42. Sadowski HB, Shuai K, Darnell JE, Jr., Gilman MZ. A common nuclear signal transduction  
732 pathway activated by growth factor and cytokine receptors. *Science* 1993; 261(5129): 1739-  
733 1744.
- 734 43. Sharma B, Iozzo RV. Transcriptional silencing of perlecan gene expression by interferon-  
735 gamma. *The Journal of biological chemistry* 1998; 273(8): 4642-4646.

- 736 44. Shuai K, Liu B. Regulation of JAK-STAT signalling in the immune system. *Nature reviews*  
737 *Immunology* 2003; 3(11): 900-911.
- 738 45. Echeverria V, Yarkov A, Aliev G. Positive modulators of the alpha7 nicotinic receptor  
739 against neuroinflammation and cognitive impairment in Alzheimer's disease. *Progress in*  
740 *neurobiology* 2016; 144: 142-157.
- 741 46. Baruch K, Rosenzweig N, Kertser A, Deczkowska A, Sharif AM, Spinrad A et al. Breaking  
742 immune tolerance by targeting Foxp3(+) regulatory T cells mitigates Alzheimer's disease  
743 pathology. *Nature communications* 2015; 6: 7967.
- 744 47. Lee YJ, Choi DY, Choi IS, Kim KH, Kim YH, Kim HM et al. Inhibitory effect of 4-O-  
745 methylhonokiol on lipopolysaccharide-induced neuroinflammation, amyloidogenesis and  
746 memory impairment via inhibition of nuclear factor-kappaB in vitro and in vivo models.  
747 *Journal of neuroinflammation* 2012; 9: 35.
- 748
- 749
- 750
- 751
- 752

753 **Figure legends**

754 **Figure 1 Overexpression of hTau activates STAT1 with an increased nuclear translocation**  
755 ***in vitro*.**

756 (A, B) Overexpression of human hTau (hTau) induced significant alterations of 9 transcription  
757 factors screened by using Transcription Factors Activation Profiling Plate Array II, in which 96  
758 transcription factors were monitored. The empty vector was transfected as a control (Ctrl).

759 (C-F) Expression of hTau (probed by HT7) increased total and the phosphorylated STAT1 at  
760 Tyr701 (pY-STAT1) in cell whole extracts (C, D) and the nuclear fraction (E, F) measured by  
761 Western blotting.

762 (G) The representative immunofluorescent images and quantitative analysis show significantly  
763 increased STAT1 signal in the nuclear fraction of HEK293 cells with overexpression of hTau  
764 compared with the empty vector control (eGFP). Scale bar, 10  $\mu\text{m}$ .

765 (H) Overexpression of hTau most significantly increased STAT1 monomer and dimer formation  
766 in nuclear fraction (Nu) measured by Western blotting.

767 (I) Overexpression of hTau increased STAT1 activity in HEK293 cells detected by luciferase  
768 assay.

769 (J) Overexpression of hTau increased STAT1-DNA binding activity in HEK293 cells measured  
770 by electrophoretic mobility shift assay (EMSA). \*, indicates STAT1/DNA complex.

771 Data were presented as mean  $\pm$ SD of at least three independent experiments (student's unpaired  
772 *t*-test). \*,  $p < 0.05$ , \*\*,  $p < 0.01$ , \*\*\*,  $p < 0.001$  vs Ctrl,

773 **Figure 2 Overexpression of hTau upregulates phosphorylated STAT1 *in vivo*.**

774 (A, B) AAV-hTau-eGFP (hTau) or the empty vector AAV-eGFP (eGFP) ( $1.13 \times 10^{13}$  v.g./ml)  
775 was stereotaxically injected into hippocampal CA3 of 3 m-old C57 mice. After one month, the  
776 increased levels of STAT1 and pY-STAT1 in hippocampal total extracts and the nuclear fraction  
777 were detected in hTau group by Western blotting.

778 (C, D) The increased STAT1 and pY-STAT1 in hippocampal total extracts and the nuclear  
779 fraction of 12 m-old hTau transgenic mice measured by Western blotting.

780 (E, F) The representative images of STAT1 and pY-STAT1 in the brain of AD patients probed  
781 by co-immunohistochemical staining and quantitative analysis (hematoxylin stains nuclei, purple;  
782 DAB stains the target proteins, brown; n=4-6 slices). Scale bar, 200  $\mu$ m, or 20  $\mu$ m for the  
783 enlarged.

784 Data were presented as mean  $\pm$  SD of at least three independent experiments (student's unpaired  
785 *t*-test). \*,  $p < 0.05$ , \*\*,  $p < 0.01$  vs eGFP or wt.

786 **Figure 3 Downregulating STAT1 ameliorates hTau-induced cognitive and synaptic**  
787 **impairments.**

788 (A, B) AAV-Cre ( $5 \times 10^{12}$  v.g./ml) mixed with AAV-hTau or AAV-eGFP ( $1.13 \times 10^{13}$  v.g./ml)  
789 were stereotaxically injected into the hippocampal CA3 of 3 m-old STAT1<sup>flx/flx</sup> mice. One  
790 month later, downregulation of STAT1 was confirmed by Western blotting and  
791 immunohistochemical staining. Scale bar, 200  $\mu$ m (left); 100  $\mu$ m (right); n=3 each group.

792 (C) Downregulation of STAT1 ameliorated hTau-induced spatial learning deficit shown by the  
793 decreased escape latency during 5 consecutive days training in Morris water maze (MWM) test  
794 (n=9-11 for each group).

795 (D-G) Downregulation of STAT1 ameliorated hTau-induced spatial memory deficit shown by  
796 the decreased latency to reach the platform quadrant (D), the increased crossing time in the  
797 platform site (E) and time spent in the target quadrant (F) measured at day 6 by removed the  
798 platform in MWM test; no motor dysfunction was seen (G) (n=9-11 for each group).

799 (H) Downregulation of STAT1 ameliorated hTau-induced contextual memory deficits measured  
800 at 24 h during fear conditioning test (n=8 each group).

801 (I-L) Downregulation of STAT1 restored slopes of field excitatory postsynaptic potential  
802 (fEPSP) with no influence on paired-pulse ratio (PPR) recorded in hippocampal CA3 of hTau or  
803 STAT1 knockdown mice (n=5 slices from 4 mice for each group).

804 (M-P) One month after the virus infection, whole cell patch clamp was used to measure the  
805 function of NMDA (at +40 mV) and AMPA (at -70 mV) receptors on acute brain slices (400  
806  $\mu\text{m}$ ). The insets show representative sample traces of EPSCs in virus infected neurons (M). The  
807 reduced NMDA and unchanged AMPA currents with a reduced NMDA/AMPA ratio were seen  
808 in hTau infected neurons, while knockdown of STAT1 restored the hTau-induced NMDA  
809 currents (N-P). (n = 12 neurons from 4 animals for eGFP group; n = 11 neurons from 4 animals  
810 for hTau group; n = 13 neurons from 4 animals for hTau+CRE group).

811 Data were presented as mean  $\pm$  s.e.m for C-H and mean  $\pm$  SD for others (two-way repeated  
812 measures analysis of variance (ANOVA) followed by Bonferroni' s post hoc test for C, two-way  
813 analysis of variance (ANOVA) followed by Bonferroni' s post hoc test for I-K, one-way analysis  
814 of variance (ANOVA) followed by Bonferroni' s post hoc test for others). \*,  $p < 0.05$ , \*\*,  $p < 0.01$ ,  
815 \*\*\*,  $p < 0.001$  vs eGFP; #,  $p < 0.05$ , ###,  $p < 0.001$  vs hTau.

816 **Figure 4 Overexpressing hTau suppresses expression of NMDARs by upregulating STAT1**  
817 **in mice.**

818 (A-C) Overexpression of AAV-hTau decreased the protein and mRNA levels of GluN1, GluN2A  
819 and GluN2B detected by Western blotting and qRT-PCR in the hippocampal CA3 of C57 mice,  
820 compared with the AAV-eGFP vector control. Data were presented as mean  $\pm$  SD (n=3-4;  
821 student's unpaired t-test).

822 (D-F) Simultaneous downregulation of STAT1 by infusing AAV-Cre in hippocampal CA3 of  
823 STAT1<sup>fllox/fllox</sup> mice abolished the hTau-induced inhibition in expression of NMDAR protein and  
824 mRNA. Data were presented as mean  $\pm$  SD (n=3-4; student's unpaired t-test).

825 \*,  $p < 0.05$ , \*\*,  $p < 0.01$ , \*\*\*,  $p < 0.001$  vs eGFP or hTau.

826 **Figure 5 Overexpressing hTau increases binding of STAT1 to NMDAR promoters and**  
827 **inhibits the expression of NMDARs.**

828 (A) Overexpression of AAV-hTau increased binding of STAT1 to the promoter regions of  
829 *GluN1*, *GluN2A* and *GluN2B* gene in hippocampal CA3 extracts measured by chromatin  
830 immunoprecipitation assay (CHIP).

831 (B) Overexpression of hTau or wildtype STAT1 (WT-STAT1) inhibits the transcription activity  
832 of NMDARs compared with the empty vector control (Ctrl) measured by luciferase activity  
833 assay in HEK293 cells.

834 (C-J) Diagrams show the predicted GAS promoter element (GASs) for STAT1 in the promoter (-  
835 2000-+299bp) of *GluN1* (C), *GluN2B* (E) and *GluN2A* (G, I). The GASs or the mutant (MUT)  
836 plasmids were co-transfected respectively with WT-STAT1 or its empty vector (Ctrl) into



837 HEK293 cells for 24 h, and then the luciferase activity was measured (right panels). N=4 for  
838 each group.

839 Data were presented as mean  $\pm$  SD (two-way analysis of variance (ANOVA) followed by  
840 Bonferroni' s post hoc test). \*,  $p<0.05$ , \*\*,  $p<0.01$ , \*\*\*,  $p<0.001$  vs Ctrl; #,  $p<0.05$ , ###,  $p<0.001$   
841 vs wildtype reporters.

842 **Figure 6 JAK2 activation mediates hTau-induced STAT1 activation.**

843 (A, B) Overexpression of hTau in HEK293 cells for 48 h increased the activity-dependent  
844 phosphorylation of JAK2, JNK1 and ERK1 compared with the empty vector control (Ctrl)  
845 measured by Western blotting (n=3).

846 (C-F) Pharmacological inhibition of ERK1 (C, D) or JNK1 (E, F) for 24 h did not significantly  
847 affect the hTau-induced STAT1 phosphorylation at pY-STAT1 (Tyr701) in total extracts (C, E)  
848 and the nuclear fraction (D, F) measured by Western blotting (n=3). The alteration of pS-STAT1  
849 (Ser727) confirms the efficacy of JNK1 inhibitors.

850 (G-J) Pharmacological inhibition of JAK2 (G, H) or knockdown JAK2 by siRNA (I, J) abolished  
851 hTau-induced STAT1 phosphorylation at Tyr701 in total extracts (G, I) and the nuclear fraction  
852 (H, J) (n=3).

853 (K, L) The phosphorylated JAK2 level increased in the hippocampus of 12 m-old hTau  
854 transgenic mice (K), and the hippocampus of C57 mice infected with AAV-hTau ( $1.13 \times 10^{13}$   
855 v.g./ml) (L).

856 Data were presented as mean  $\pm$  SD (student' s unpaired *t*-test); \*,  $p<0.05$ , \*\*,  $p<0.01$  vs Ctrl,  
857 eGFP or WT.

858 **Figure 7 Blocking STAT1 activation rescues hTau-induced synapse and memory**  
859 **impairments.**

860 (A-E) AAV-eGFP (eGFP) or AAV-hTau-eGFP (hTau) ( $1.13 \times 10^{13}$  v.g./ml) or AAV-Y701F-  
861 STAT1 ( $5 \times 10^{12}$  v.g./ml) or AAV-Y701F-STAT1 ( $5 \times 10^{12}$  v.g./ml) plus hTau was stereotaxically  
862 injected into hippocampal CA3 of 3 m-old C57 mice. After one month, learning and memory  
863 were detected by MWM test.

864 (A) The representative fluorescence image confirms expression of AAV-hTau and AAV-Y701F-  
865 STAT1.

866 (B) Overexpression of Y701F-STAT1 mitigated hTau-induced spatial learning deficits shown by  
867 the decreased escape latency during water maze training. Data were presented as mean  $\pm$  s.e.m  
868 (n=7-10 each group, two-way analysis of ANOVA, Bonferroni's post hoc test).

869 (C-E) Overexpression of Y701F-STAT1 mitigated hTau-induced spatial memory impairment  
870 shown by the decreased latency to reach the platform (C), the increased crossing time in the  
871 platform site (D) and time spent in the target quadrant (E) measured at day 6 by removed the  
872 platform (n=7-10 each group). Data were presented as mean  $\pm$  s.e.m (two-way ANOVA,  
873 Bonferroni's post hoc test).

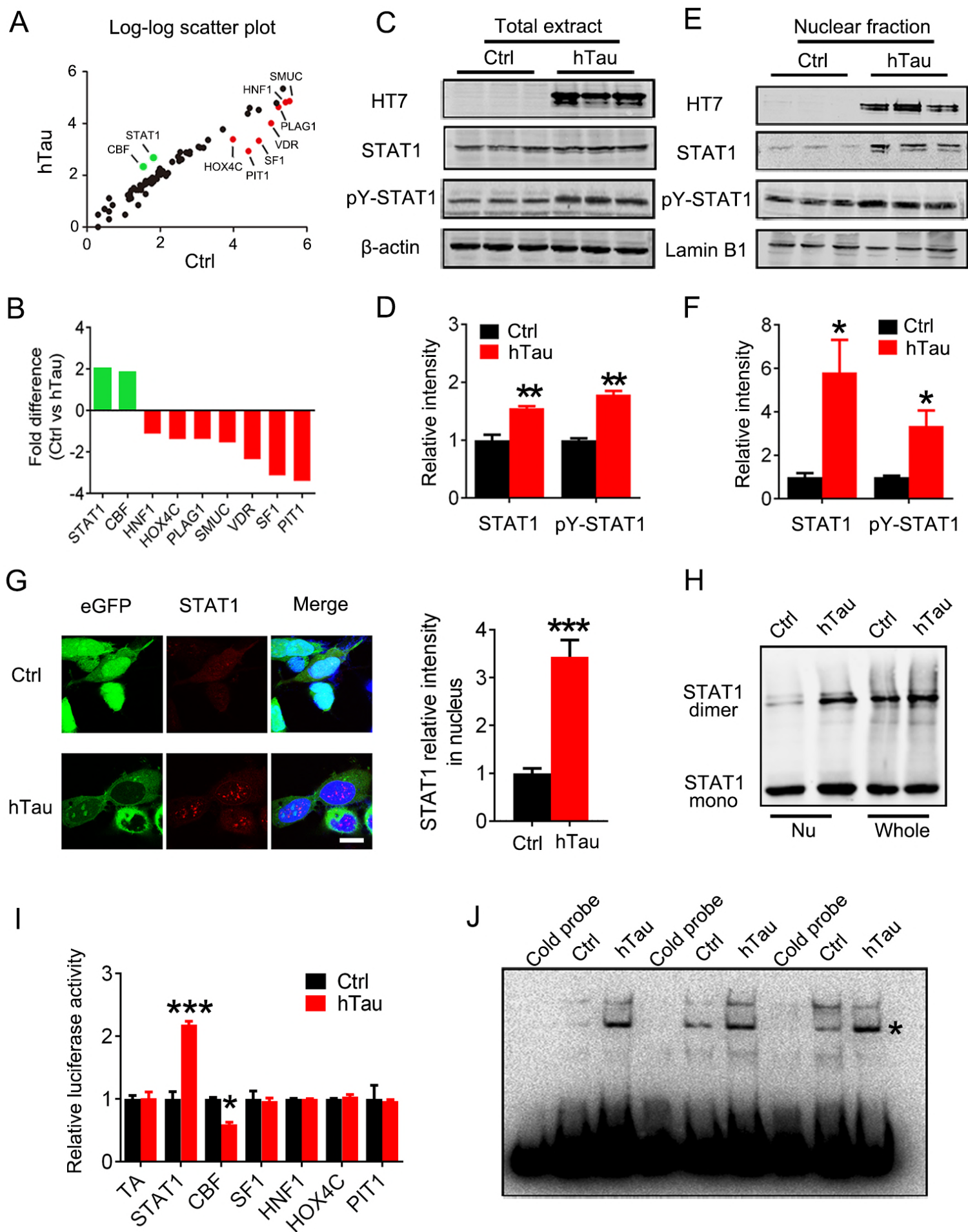
874 (F) Expression of Y701F-STAT1 did not change the swimming speed of the mice in water maze  
875 task.

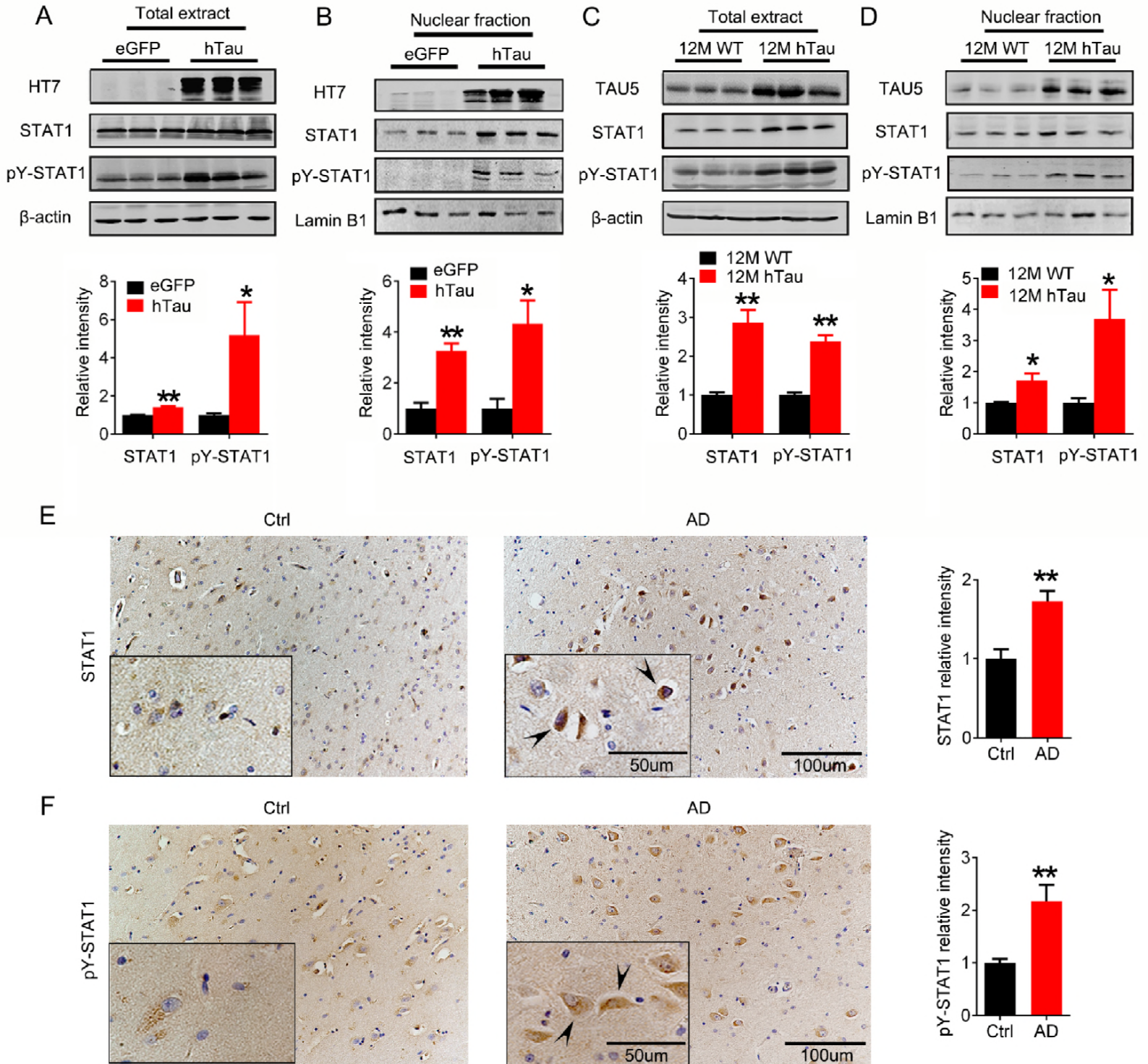
876 (G) Simultaneous expression of Y701F-STAT1 did not induced any further change on basal  
877 synaptic transmission (I/O curve) compared with expression of hTau alone, recorded in  
878 hippocampal CA3 (n=5 slices from 4 mice for each group).

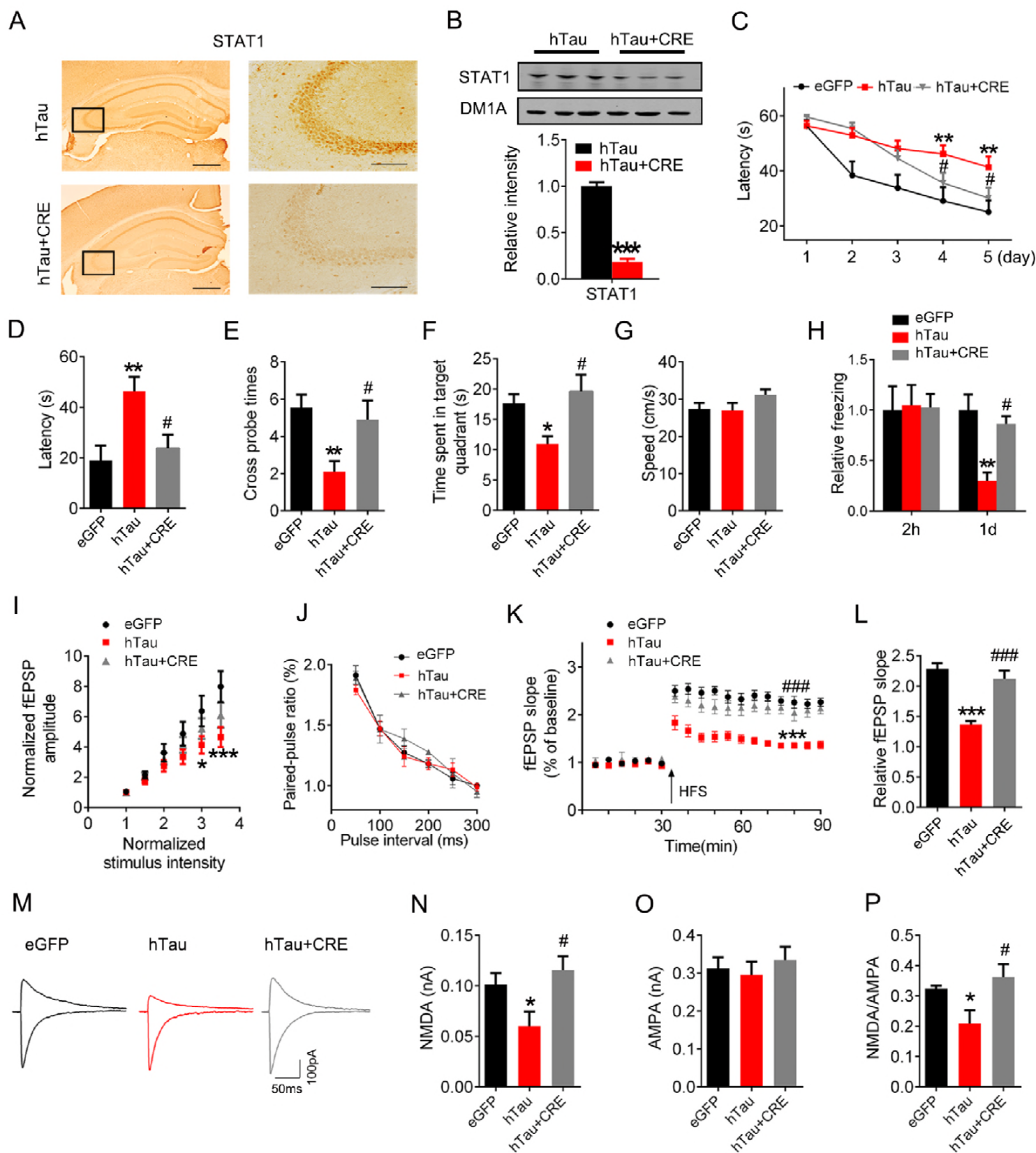
879 (H) Simultaneous expression of Y701F-STAT1 abolished the hTau-induced inhibition of field  
880 excitatory postsynaptic potential (fEPSP), recorded in hippocampal CA3 of C57 mice (student's  
881 unpaired t-test, n=5 slices from 4 mice for each group).

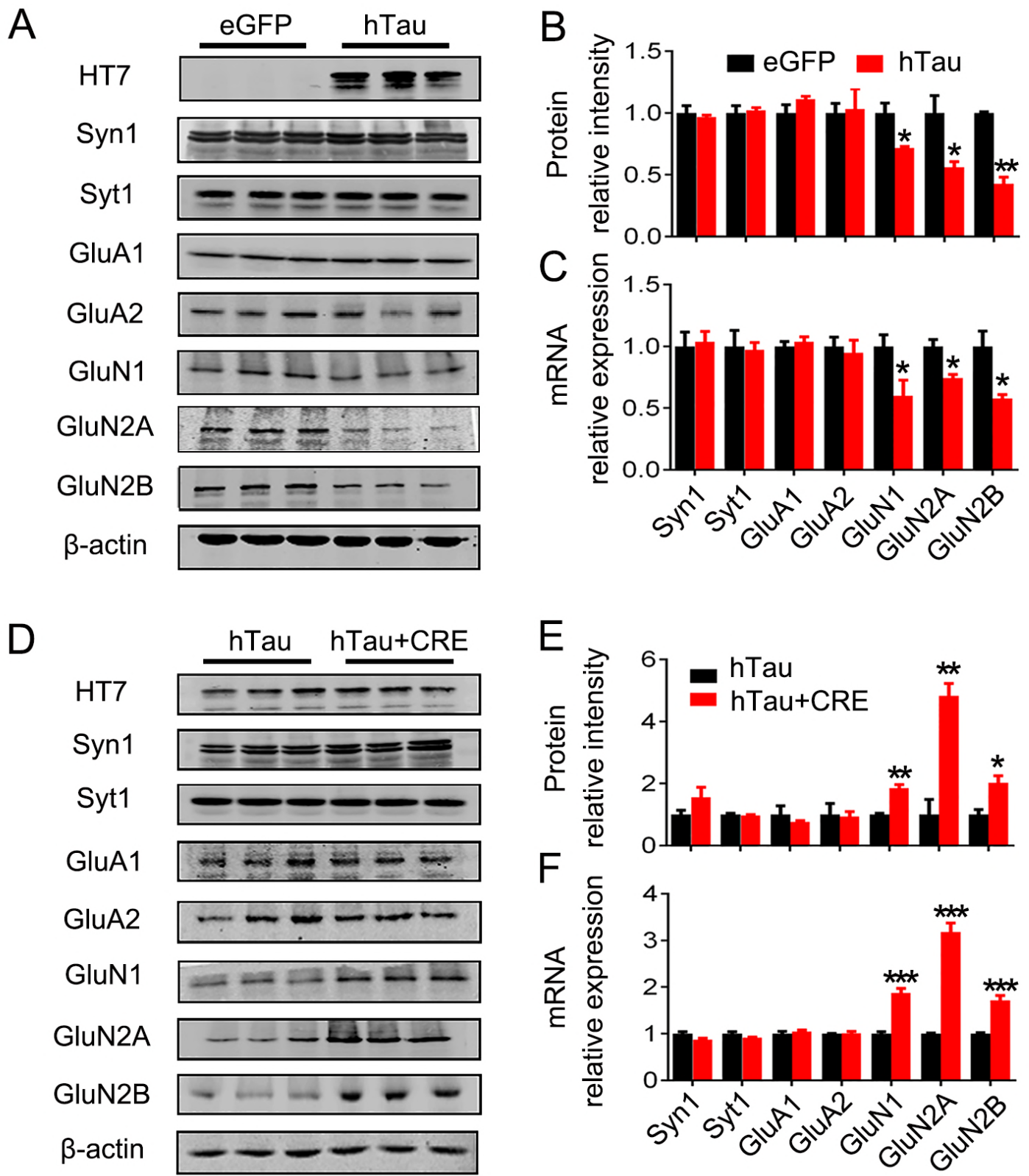
882 (I-K) Simultaneous expression of Y701F-STAT1 rescued the hTau-induced suppression of  
883 NMDARs protein (I, J) and mRNA (K) expression measured by Western blotting and qRT-PCR  
884 in hippocampal CA3 of C57 mice.

885 Data were presented as mean  $\pm$  s.e.m for B-F and mean  $\pm$  SD for others (two-way repeated  
886 measures analysis of variance (ANOVA) followed by Bonferroni's post hoc test for B, two-way  
887 analysis of variance (ANOVA) followed by Bonferroni's post hoc test for others, N=3 each  
888 group). \*,  $p < 0.05$ ; \*\*,  $p < 0.01$  vs eGFP or hTau; #,  $p < 0.05$ , ##,  $p < 0.01$  vs hTau.

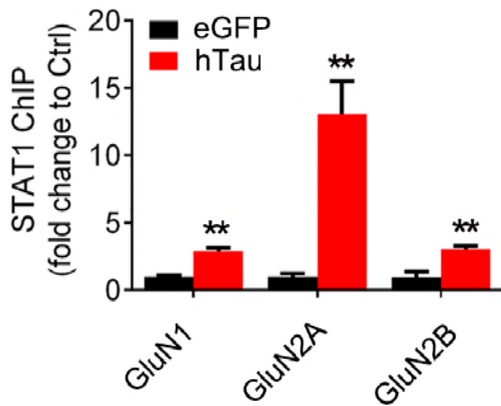




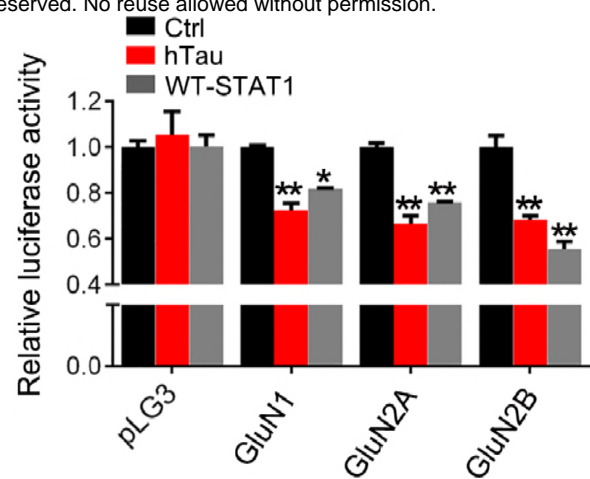




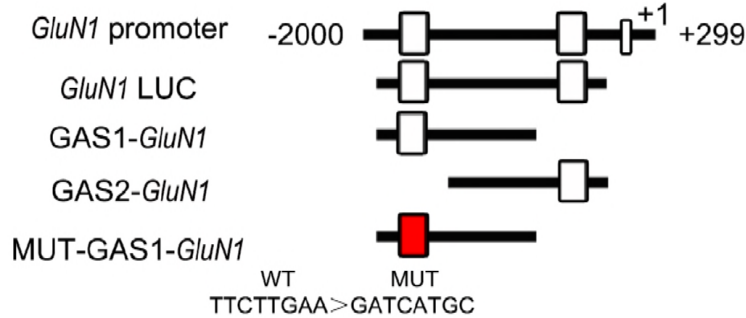
**A**



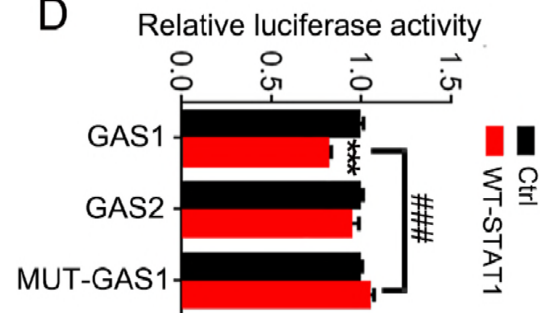
**B**



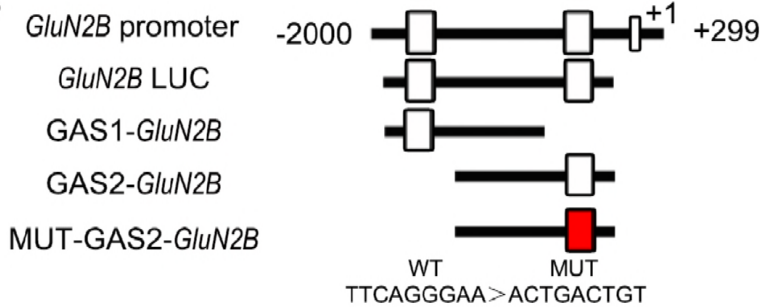
**C**



**D**



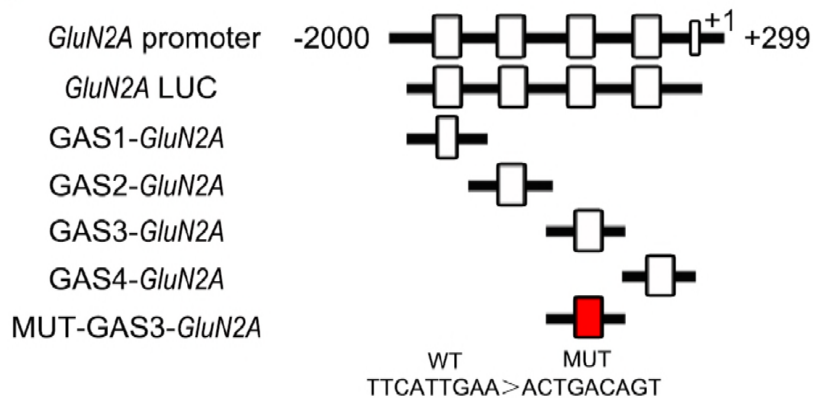
**E**



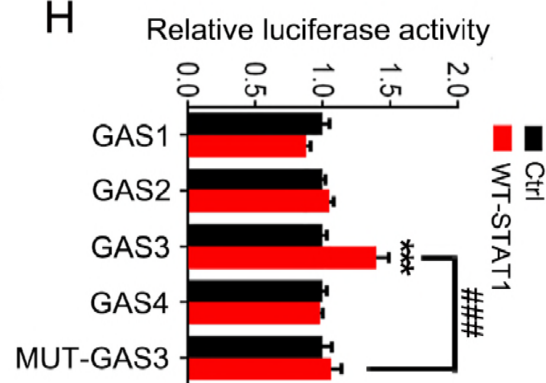
**F**



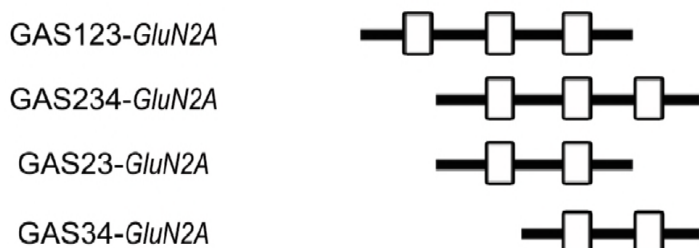
**G**



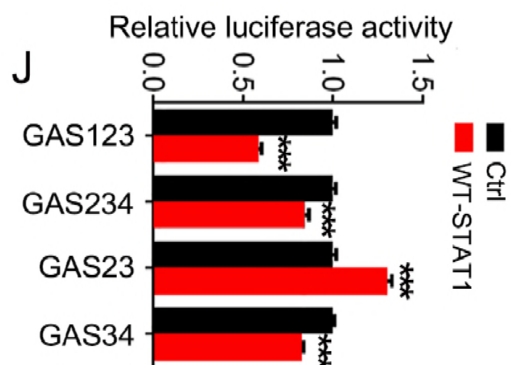
**H**



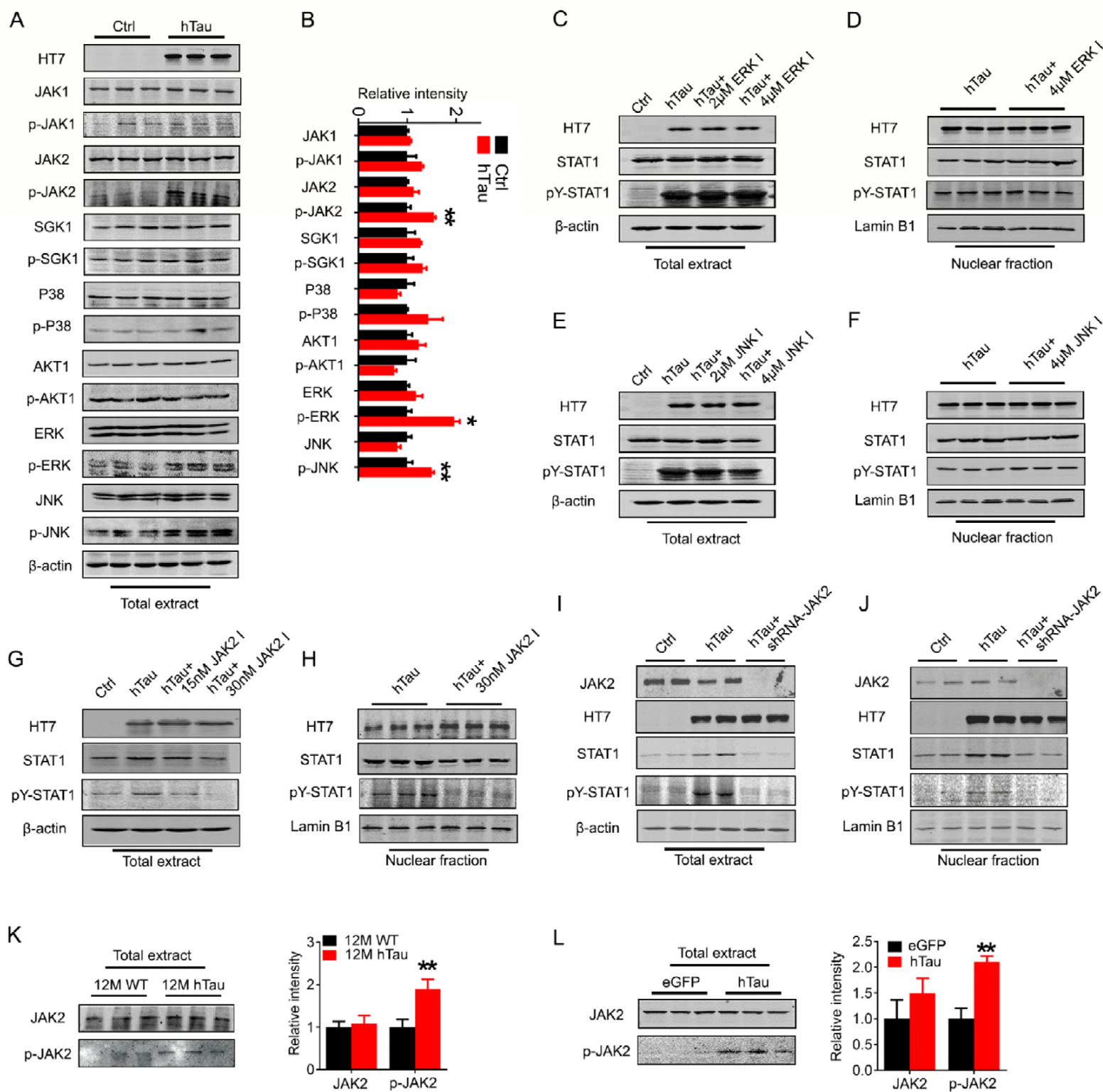
**I**



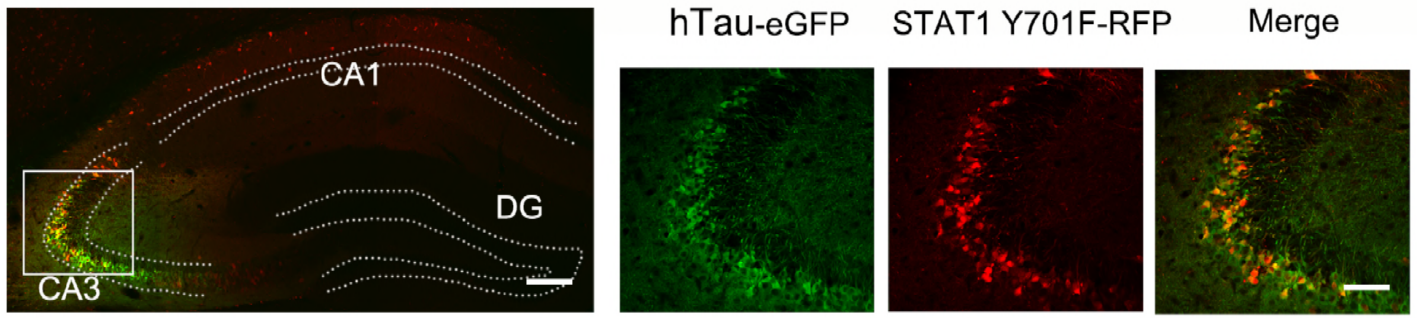
**J**



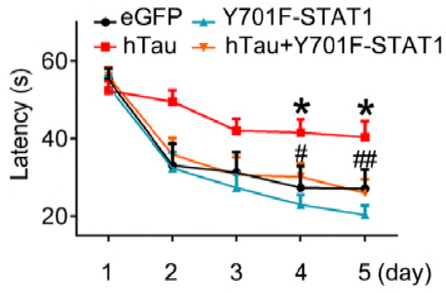




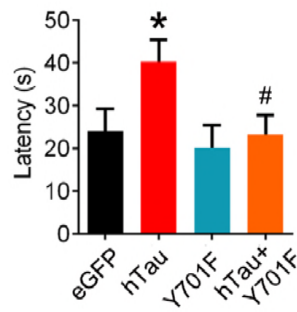
A



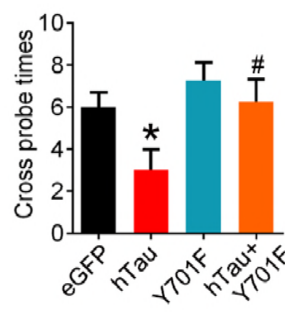
B



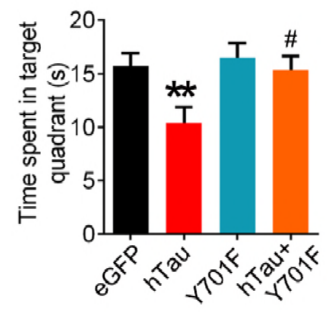
C



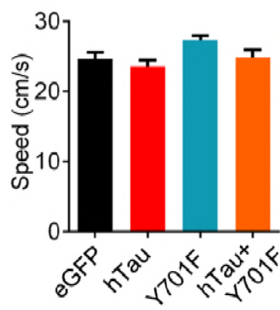
D



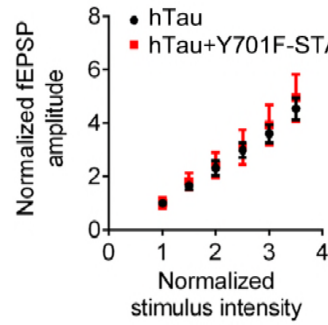
E



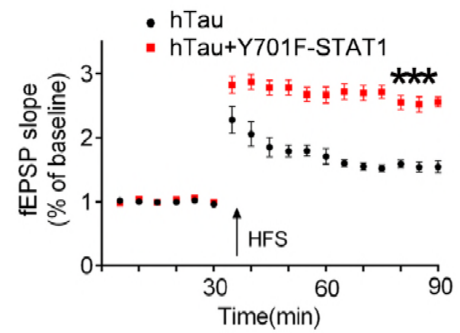
F



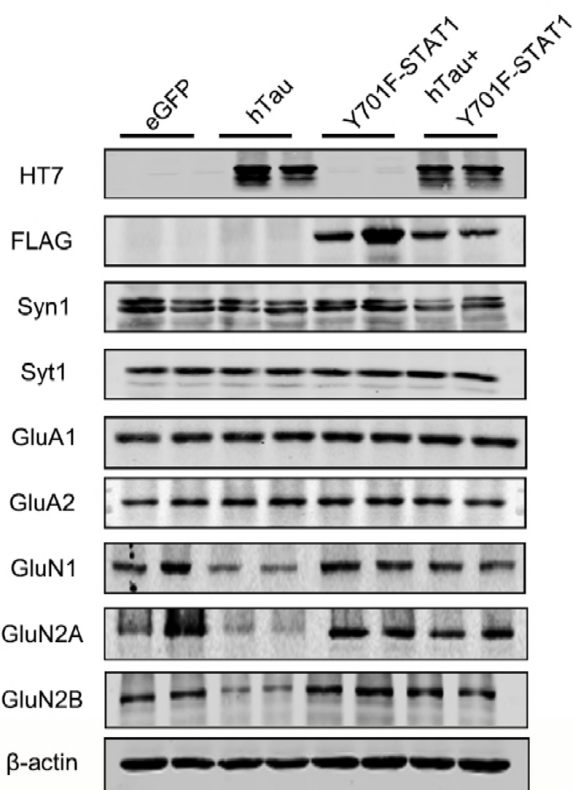
G



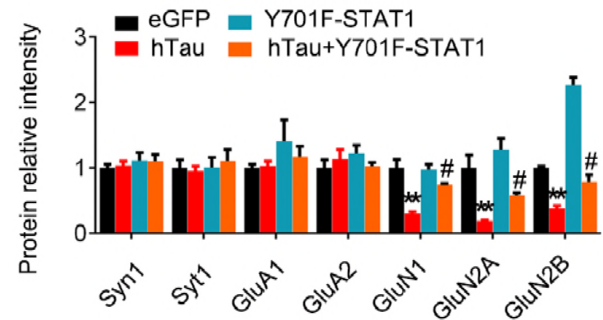
H



I



J



K

